PHYSICAL REVIEW A VOLUME 32, NUMBER 6 DECEMBER 1985

Thermal convection under external modulation of the driving force. I. The Lorenz model

Guenter Ahlers
Department of Physics, University of California, Santa Barbara, California 93106

P. C. Hohenberg
AT&T Bell Laboratories, Murray Hill, New Jersey 07974

M. Lücke
Institut für Theoretische Physik, Universität des Saarlandes, D-6600 Saarbrücken, West Germany and Institut für Festkörperforschung der Kernforschungsanlage Jülich, D-5170, Jülich, West Germany*
(Received 14 June 1985)

Thermal convection between horizontal plates is considered for a situation in which the driving force varies periodically in time. This variation may come from changes in the temperature of the plates or from a vertical oscillation of the cell, causing variation of the gravitational force. Truncation of the Boussinesq equations leads to a three-mode model which is a generalization of the Lorenz model to the case of external modulation. Similar models have previously been introduced by Finucane and Kelly for stress-free horizontal boundaries and by Gresho and Sani for the rigid-boundary case. The threshold behavior is that of a parametrically driven damped oscillator, whose bifurcations are studied numerically, as well as analytically in certain limits. It is found that in general the modulation stabilizes the conducting state. For stress-free horizontal boundaries the threshold shifts predicted by the model coincide with the results of Rosenblat and Herbert in the limit of low frequency and agree well with Venezian's results for small modulation amplitude, both obtained using the full Boussinesq equations. For rigid boundaries the results agree well with numerical calculations of Rosenblat and Tanaka. The nonlinear behavior of the model is also studied, and the convective contribution to the heat current evaluated. The Lorenz model is shown to reproduce, either exactly or to a good approximation, most previous theoretical results on modulated convection, and the model can be studied simply for a wide range of parameters. The above discussion refers to a laterally infinite system. For a real finite system, sidewall effects are shown to cause a rounding of the convective threshold in the presence of modulation, particularly at low frequencies. A calculation of these effects is carried out within the framework of the Lorenz truncation, and the resulting imperfect bifurcation of the model is studied numerically. In a companion paper (immediately following this one) quantitative experimental results are presented and compared to the predictions of the Lorenz model.

I. INTRODUCTION

The stability of periodic states of hydrodynamical systems is a subject of considerable interest. A particular subclass of problems concerns systems under periodic external modulation, whose amplitude and frequency can be varied independently. Interest in this field was originally stimulated by the experimental work of Donnelly, Reif, and Suhl[1] on modulated Couette-Taylor flow (see also Donnelly[2]). The present paper concerns itself with the theory of Rayleigh-Bénard convection, in which either the temperature of the gravitational force is externally modulated. A subsequent paper[3] will describe quantitative experiments and compare their results with the theory.

The subject of modulated convection has received considerable theoretical attention (for a review see Davis[4]), but only little experimental interest.[5,6] The theoretical work deals mainly with the problem of stability, for which various criteria have been proposed.[4] The first is "monotonic stability" which means that every disturbance decays at all times. Secondly there is "transient stability" in which disturbances experience net decay over a cycle, but can grow during part of the cycle. A third form of stability, determined by an "amplitude criterion"[7] requires that disturbance amplitudes remain within a specified factor of their initial values. Most of the theoretical work has involved the calculation of stability thresholds according to these different criteria, for various forms of external modulation and different values of the fluid parameters. Very little work has been devoted to the behavior above threshold, e.g., to a comparison of the heat transport with and without modulation.

The main purpose of the present work is to derive a model which is sufficiently accurate to reproduce the main features of the full hydrodynamic problem, yet sufficiently simple to allow detailed quantitative evaluation and comparison with experiment. Our model is a generalization of the equations of Lorenz[8,9] to situations with

 ©1985 The American Physical Society

external temperature or gravity modulation (the two cases yield somewhat different equations) for both stress-free and rigid horizontal boundary conditions. The model therefore consists of three coupled ordinary differential equations with time-dependent coefficients which depend on the nature of the horizontal boundaries. These nonlinear equations can be solved numerically in a straightforward manner, and a number of properties at or near threshold can be calculated analytically. A preliminary account of the results was presented earlier.[10,11]

Since the Lorenz model is not exact above threshold even in the absence of modulation it can hardly be expected to describe the behavior in the presence of modulation with complete accuracy. We may note, however, that the model does predict the exact value of the threshold, as well as the exact slope of the Nusselt number above threshold, for stress-free horizontal boundaries in the absence of modulation. Moreover, for $R \lesssim 2R_c$ the model yields qualitatively correct answers since the system is in a state of steady convection in that case. It should also be stated that our model as well as most earlier treatments neglect the possibility of a change in horizontal wave vector, or in convection pattern, brought about by the modulation. Recently, Roppo, Davis, and Rosenblat[12] have predicted that for an ideal laterally infinite system, modulation produces a subcritical bifurcation to a hexagon pattern very near threshold. However, recent flow visualization experiments[13] have shown that sidewall forcing which occurs in real systems tends to favor a roll pattern and to suppress the hexagon solution. This means that the assumption of a convection pattern unchanged by the modulation is a reasonable approximation in practice. Nevertheless, in view of the above-mentioned limitations of the Lorenz model we shall confine our investigation of the modulated case to the region near the threshold. This means in particular that we shall be well below the range $R/R_c > 20$, where the model shows chaotic solutions[8] in the absence of modulation.

The threshold behavior of the model reduces to that of a parametrically modulated damped oscillator representing the most unstable Fourier mode $x(t)$ of the velocity field,

$$m\ddot{x} + m\Gamma\dot{x} - \tilde{\epsilon}(t)x = 0 , \tag{1.1}$$

where

$$\tilde{\epsilon}(t) = \epsilon + \tilde{\delta}\cos(\omega t) . \tag{1.2}$$

Here ϵ is the relative deviation of the mean Rayleigh number R from its critical value $R_c^{\rm stat}$ in the absence of modulation,

$$\epsilon = (R - R_c^{\rm stat})/R_c^{\rm stat} . \tag{1.3}$$

For stress-free horizontal boundaries $m = 4/9\pi^4\sigma$, and $\Gamma = 3\pi^2(\sigma+1)/2$, where σ is the Prandtl number, ω the modulation frequency, and $\tilde{\delta}$ is determined by the amplitude of external modulation. The stability threshold ϵ_c for bifurcation from the conductive state $x=0$ to a periodic solution $x(t)$ can be evaluated numerically, and analytically in certain limits ($\tilde{\delta}\to 0$ or $\omega\to 0$). If the cosine is replaced by a step-function modulation, a general analytic formula[14] exists for $\epsilon_c(\tilde{\delta},\omega)$. The results show that external modulation *stabilizes* the conductive state ($\epsilon_c > 0$), unless $\tilde{\delta}$ is quite large ($\tilde{\delta} \gtrsim 3$) at which point the Lorenz truncation ceases to be a reasonable approximation. As explained in detail below, the threshold ϵ_c of Eq. (1.1) coincides for $\omega\to 0$ with the result of Rosenblat and Herbert[7] and of Dowden,[15] obtained for the full Boussinesq equations with stress-free horizontal boundaries. Furthermore, ϵ_c as a function of σ and ω agrees very well for small modulation amplitude with the calculations of Venezian[16] performed to second order, also for the full Boussinesq equations with free boundaries. Similarly, the generalization of (1.1) to rigid boundaries (see Gresho and Sani[17]) leads to excellent agreement with numerical results of Rosenblat and Tanaka.[18] We may therefore assert that the Lorenz model yields a (transient) stability threshold which reproduces all previous work, either exactly or to good approximation.

The nonlinear behavior of the model is reasonably well represented by the damped parametrically modulated anharmonic oscillator (see Davis and Rosenblat[19] and Gresho and Sani[17])

$$m\ddot{x} + m\Gamma\dot{x} - \tilde{\epsilon}(t)x + x^3 = 0 , \tag{1.4}$$

where the convective current (normalized by R_c) is given by

$$j^{\rm conv}(t) \simeq g^{-1}x^2(t) , \tag{1.5}$$

with $g^{-1}=2$ for stress-free horizontal boundaries. For ϵ just above the threshold ϵ_c, the solution of (1.4) can be obtained by a perturbation theory, whose domain of validity is shown to be $\epsilon - \epsilon_c \ll \omega$, independent of $\omega/\tilde{\delta}$ (see Appendix C). The perturbation expansion allows us to give analytic expressions for the slope of the average convective current $\langle j^{\rm conv}\rangle$ versus $\epsilon-\epsilon_c$, as a function of ω and Prandtl number σ, to lowest order in the modulation amplitude $\tilde{\delta}$. In addition, for low frequencies and sufficiently far from threshold ($\epsilon > \tilde{\delta}$), one can carry out an adiabatic expansion of (1.4) to obtain an expression for $x(t)$ as a power series in ω. The threshold behavior, on the other hand, does not simplify significantly at low frequencies.

The amplitude equation

$$m\Gamma\dot{x} - \tilde{\epsilon}(t)x + x^3 = 0 , \tag{1.6}$$

obtained by neglecting the $\ddot{x}$ term in (1.4), has a threshold which vanishes identically for all ω and $\tilde{\delta}$. [Equations (1.4) and (1.6) only agree in the limit $\sigma\to\infty$.[20]] The amplitude equation (1.6) gives the correct initial slope of the Nusselt number in the absence of modulation, and it describes the experimental behavior near threshold accurately in that case, as discussed for example by Ahlers *et al.*[21] These authors showed that the time scale for the onset of convection when the Rayleigh number is raised from below to above R_c could be accounted for by a small forcing term on the right-hand side of Eq. (1.6). The physical origin of this term was not completely elucidated by Ahlers *et al.*,[21] but they suggested that possible contributions are sample imperfections, time-dependent sidewall heating, and various noise and fluctuation effects in the experiment (the contribution of microscopic thermal fluctuations in the fluid was also considered and turned out to be many times smaller than was needed to explain the ob-

served onset times). In a subsequent paper Cross *et al.*[22] showed that a time-dependent Rayleigh number gives rise to a term

$$\xi(t)=\xi_1\dot{R}(t)/R_c^{\text{stat}} \tag{1.7}$$

added to the right-hand side (rhs) of Eq. (1.6), which describes a roll pattern parallel to the sidewall. The calculated strength ξ_1 and the frequency dependence of (1.7) agreed remarkably well with the experimental results of Ahlers *et al.*,[21] with no adjustable parameters.

A calculation similar to that of Cross *et al.*[22] is carried out here in the framework of the Lorenz truncation. It yields a forcing term similar to (1.7) on the rhs of Eq. (1.4). In the presence of this inhomogeneous term, the nonlinear oscillator no longer has a sharp bifurcation [at least for $\dot{R}(t)\neq 0$]. One can then define an effective threshold by determining the value of ϵ at which the reduced convective current averaged over a period reaches a specified value (0.01, say). This threshold is analogous to the one obtained from the amplitude criterion of Rosenblat and Herbert[7] mentioned above, but its definition depends on the physical processes responsible for the onset of convection, rather than on some arbitrary choice of initial value. In particular, the calculation of Cross *et al.*[22] predicts that if the top and bottom plates are modulated out of phase, then ξ_1 in Eq. (1.7) vanishes, and the threshold behavior will be drastically modified at low frequencies.

The forcing ξ will lead to an onset time τ_{on} for the growth of the convecting state. In the modulation experiment this time will depend on ω and $\tilde{\delta}$, and the quantity $\omega\tau_{\text{on}}(\sigma,\omega)$ will determine the importance of the forcing ξ. At low frequencies, $\omega\tau_{\text{on}}<1$, convection has enough time to grow to appreciable size during the supercritical part of the period where $R(t)>R_c^{\text{stat}}$. Thus, the stabilization of conduction ($\epsilon_c>0$) found for the ideal system will not take place, since it depends on a delicate cancellation of growth and decay during a period. This cancellation is hindered by the forcing ξ which sets a lower limit on the value of x during the cycle. For high frequencies, $\omega\tau_{\text{on}}>1$, convection does not grow appreciably during a period of oscillation unless one is above the threshold of the ideal system, so the forcing is unimportant in determining the actual threshold. The two cases $\omega\tau_{\text{on}}<1$ and $\omega\tau_{\text{on}}>1$ correspond roughly to the ranges of applicability of the amplitude criterion and the transient stability criterion, respectively. In any case, the precise definition of a stability criterion is unnecessary, since the present theory calculates the experimentally observed quantities directly.

An interesting effect of the forcing is that it breaks the symmetry between the two solutions $\pm x(t)$ of Eq. (1.4), and that it may cause transitions between them as the amplitude or frequency of the forcing are varied, since the solution with the proper phase relationship with $\xi(t)$ is favored. If the system starts out in the unfavored orbit, it will eventually come close enough to $x=0$ so that even a very small value of ξ will cause the transition. This effect will be discussed below, and demonstrated experimentally in paper II.

Another consequence of the forcing appears to be the suppression of the subcritical bifurcation to a hexagon pattern predicted recently by Roppo *et al.*[12] for an ideal system. Although we cannot demonstrate this effect theoretically, flow visualization experiments by Steinberg *et al.*[13] show that for moderate aspect ratios ($L\lesssim 7.5$) convection first appears in a roll pattern in the modulated case. These findings seem to us to justify the use of the Lorenz model (which assumes the same convection pattern with and without modulation) to analyze experiments in small systems.

For the case of Taylor-Couette flow a detailed theoretical treatment by Hall[23] led to a destabilizing effect of modulation ($\epsilon_0<0$). To linear order in the modulation strength, Hall found an amplitude equation which is precisely (1.6), with zero threshold shift, but higher orders in $\tilde{\delta}$ led to a negative shift. Such an effect could result from a negative mass m in Eq. (1.4), but stability then requires higher-order derivatives as well. It is therefore an interesting open problem to find a truncated set of equations which approximates the Taylor-Couette system under modulation as well as the Lorenz model does for the convection case.

Section II contains a derivation of the Lorenz model for a laterally infinite system for both temperature and gravity modulation. The truncation of the Boussinesq equations to three modes is of course uncontrolled, but once that approximation has been made the subsequent derivation follows exactly. Section III examines the threshold for the ideal (laterally infinite) model, both analytically and numerically, and compares the results to previous work. In Sec. IV the nonlinear behavior immediately above threshold is studied, analytically via perturbation theory, as well as numerically. The effect of sidewalls is considered in Sec. V, where it is shown that the time dependence of the heating causes an inhomogeneous forcing of the equations and leads to an imperfect bifurcation. Many of the detailed calculations are given in the Appendixes.

II. THE MODEL

We consider a fluid placed between horizontal plates extending laterally to infinity. The modifications to the model introduced by the sidewalls will be considered in Sec. V below. Let the Rayleigh number

$$R(t)=[T^l(t)-T^u(t)]g(t)d^3\alpha/\nu\kappa \tag{2.1}$$

be modulated periodically in time either by varying the temperatures $T^l(t)$ and $T^u(t)$ of the lower and the upper plates plates, respectively, or by oscillating the whole cell up and down, thus varying the acceleration $g(t)$ around its mean $\langle g(t)\rangle=g$, the gravitational acceleration. In the above formula d is the plate separation, α the thermal expansion coefficient, ν the kinematic viscosity, and κ the thermal diffusivity of the fluid. In the following we shall use dimensionless quantities obtained by scaling lengths, times, temperatures, and pressures by d, d^2/κ, $\kappa\nu/\alpha g d^3$, and $\rho\kappa^2/d^2$, respectively, with ρ the mean fluid density.

The Oberbeck-Boussinesq equations for the system with Prandtl number $\sigma=\nu/\kappa$ are

$$\partial_t u_i = -[(\mathbf{u}\cdot\nabla)u_i + \nabla_i p] + \sigma\nabla^2 u_i + \delta_{i,3}\sigma[g(t)/g](T^{\rm cond}+\theta) , \tag{2.2a}$$

$$\partial_t \theta = \nabla^2\theta - (\mathbf{u}\cdot\nabla)(T^{\rm cond}+\theta) , \tag{2.2b}$$

$$\nabla\cdot\mathbf{u}=0 , \tag{2.2c}$$

where $\mathbf{u}(\mathbf{x},t)$ is the velocity field, p is the pressure, and the dimensionless temperature $T(\mathbf{x},t)=T^{\rm cond}(\mathbf{x},t)+\theta(\mathbf{x},t)$ is expressed in terms of the conduction field $T^{\rm cond}$ and the contribution θ due to convection. The position vector $\mathbf{x}$ has components x_1,x_2,x_3.

The conduction profile $T^{\rm cond}(\mathbf{x},t)$ satisfies the heat diffusion equation

$$(\partial_t-\nabla^2)T^{\rm cond}(\mathbf{x},t)=0 , \tag{2.3}$$

with boundary conditions

$$T^{\rm cond}(x_3=0,t)=T^l(t) , \tag{2.4a}$$

$$T^{\rm cond}(x_3=1,t)=T^u(t) . \tag{2.4b}$$

A. Temperature modulation and stress-free horizontal boundaries

We first derive the Lorenz model for a fluid layer under constant gravity, i.e., $g(t)=g$. For a periodic time variation of $T^l(t)$ and/or $T^u(t)$, the heat equation (2.3) can be solved exactly (cf. Appendixes A and D) to yield

$$T^{\rm cond}(\mathbf{x},t)-T^u(t)=R(t)(1-x_3)+S(\mathbf{x},t) , \tag{2.5}$$

in terms of an instantaneous Rayleigh number

$$R(t)=T^l(t)-T^u(t) \tag{2.6}$$

multiplying a linear profile, and a deviation $S(\mathbf{x},t)$. Note that even in the absence of lateral sidewalls the conductive temperature profile is nonlinear. The deviation $S^\infty(\mathbf{x},t)$, for the laterally infinite case, depends only on the vertical coordinate x_3 [see Eq. (A4)]; it describes temperature oscillations around the linear profile and is caused by heat "waves." The horizontal boundary conditions on the fluid velocity are assumed to be stress free [Eq. (A15)]. In the presence of convection the system (2.2) is of course highly complicated, and we shall make a drastic simplification at the outset. In Appendix A we expand Eq. (2.2) in a set of normal modes compatible with the stress-free horizontal boundary conditions, and in analogy to the derivation of the standard Lorenz model[8,9] we retain only one velocity mode (x) and two convective temperature modes (y,z). We thus arrive at the system of ordinary differential equations

$$\tau_1\frac{dx}{dt} = -\tilde\sigma[x(t)-y(t)] , \tag{2.7a}$$

$$\tau_1\frac{dy}{dt} = -y(t)+[\tilde r(t)-z(t)]x(t) , \tag{2.7b}$$

$$\tau_1\frac{dz}{dt} = -b[z(t)-x(t)y(t)] . \tag{2.7c}$$

For the present case of stress-free horizontal boundaries we have

$$b=b_f=\tfrac{8}{3} , \tag{2.8a}$$

$$\tilde\sigma=\tilde\sigma_f=\sigma , \tag{2.8b}$$

$$\tau_1=\tau_1^f=2/3\pi^2 , \tag{2.9}$$

where $\sigma=\nu/\kappa$ is the Prandtl number and

$$\tilde r(t)=\tilde r_f(t)=r(t)-2\pi\hat S^\infty(n_3=2,t)/R_c^{\rm stat} . \tag{2.10}$$

In Eq. (2.10) there enter two driving mechanisms. First and most importantly

$$r(t)=R(t)/R_c^{\rm stat} \tag{2.11}$$

is the actual Rayleigh number (2.6), divided by the critical value $R_c^{\rm stat}$ for the onset of convection in the absence of modulation. The other term is $\hat S^\infty(n_3=2,t)$, the $n_3=2$ spatial Fourier mode of the nonlinear conductive temperature profile $S^\infty(x_3,t)$ [see Eqs. (A4) and (A8)]. For a purely sinusoidal variation of the Rayleigh number

$$r(t)=r_0{\rm Re}(1+\Delta e^{-i\omega t}) \tag{2.12}$$

around a mean

$$\langle r(t)\rangle = r_0=\epsilon+1 , \tag{2.13}$$

one obtains (see Appendix A)

$$\tilde r(t)=r_0{\rm Re}[1+\tilde\Delta(\omega)e^{-i\omega t}] , \tag{2.14}$$

$$\tilde\Delta(\omega)=\tilde\Delta_f(\omega)=4\pi^2\Delta/(4\pi^2-i\omega) . \tag{2.15}$$

Note however that our formalism is not restricted to purely harmonic modulation [cf. Appendixes A and D and paper II (Ref. 3)].

Within the Lorenz model the convective contribution to the vertical heat current at the lower plate averaged over lateral dimensions and normalized by $R_c^{\rm stat}$ is determined by $z(t)$ (see Appendix A),

$$j^{\rm conv}(t)=g^{-1}z(t) , \tag{2.16}$$

where, again for stress-free boundaries,

$$g^{-1}=g_f^{-1}=2 . \tag{2.17}$$

In the absence of modulation we have $\tilde r(t)=r_0=$const (the conductive temperature profile is linear, i.e, $S\equiv 0$) and (2.7) reduces to the usual Lorenz model[8] with a bifurcation at $r_0=1$ from the conducting state ($x=y=z=0$) to the convecting state with $x=y=\pm\sqrt{z}=\pm\sqrt{r_0-1}$. In the presence of periodic modulation the bifurcations and temporal behavior will be quite different: The conductive state $x=y=z=0$ bifurcates into a time-dependent convective state where $x(t),y(t),z(t)$ are periodic functions of time. In particular the convective current given in our model by Eq. (2.16), is periodically varying above threshold. While the time averages $\langle x(t)\rangle=\langle y(t)\rangle$ and $\langle x(t)y(t)\rangle=\langle x^2(t)\rangle=\langle z(t)\rangle$ remain related to each other in a way similar to the fixed-point relations in the absence of modulation, the dependence on r_0 is changed in general. Note that the mean convective current is always positive since $\langle z(t)\rangle=\langle x^2(t)\rangle$.

B. Mechanical analogue

The Lorenz model can be rewritten[24] purely in terms of $x(t)$,

$$m\ddot{x}+m\Gamma\dot{x}=-\frac{\partial U(x,t)}{\partial x}-xM[x]\ , \tag{2.18}$$

and may then be interpreted as a mechanical system describing the motion of a particle of mass

$$m=\tau_1^2/\tilde{\sigma} \tag{2.19}$$

with friction

$$\Gamma=(\tilde{\sigma}+1)/\tau_1 \tag{2.20}$$

in a parametrically modulated potential

$$U(x,t)=\tfrac{1}{2}[1-\tilde{r}(t)]x^2+\tfrac{1}{4}x^4\ . \tag{2.21}$$

The memory effect in the internally generated force $xM[x]$ arises from integrating out the z degree of freedom in (2.7):

$$z(t)=x^2+M[x]\ , \tag{2.22}$$

$$M[x]=(b/\tau_1)(1-b/2\tilde{\sigma})\times\int_0^\infty dt'\exp(-bt'/\tau_1)[x^2(t-t')-x^2(t)]\ . \tag{2.23}$$

For the parameter values relevant to the experiments[3] one may verify numerically that close to the convective threshold $z(t)\simeq x^2(t)$, so that M may be ignored. Unless otherwise noted, however, our numerical results are based on the full Lorenz model [Eqs. (2.7) or (2.18)].

C. Relation to amplitude equation

In the absence of modulation and for Rayleigh numbers near threshold ($|r_0-1|\ll 1$), the second derivative term in (2.18) is negligible, as well as $M[x]$ [Eq. (2.23)], and the Lorenz model reduces to the amplitude equation

$$\tau_0\dot{x}(t)-\epsilon x(t)+x^3(t)=0\ , \tag{2.24}$$

with

$$\tau_0=m\Gamma=[(\tilde{\sigma}+1)/\tilde{\sigma}]\tau_1\ , \tag{2.25}$$

$$j^{\rm conv}(t)=g^{-1}x^2(t)\ . \tag{2.26}$$

For stress-free horizontal boundaries

$$\tau_0=\tau_0^f=[(\sigma+1)/\sigma]\tau_1^f=2(\sigma+1)/3\pi^2\sigma\ , \tag{2.27}$$

$g=g_f$ is given by Eq. (2.17), and Eq. (2.24) is the exact equation[25,21] near threshold for states with wave vector k_c, leading to the correct slope of the Nusselt number N for free horizontal boundary conditions and $R>R_c^{\rm stat}$,

$$(N-1)R/R_c^{\rm stat}=\langle j^{\rm conv}(t)\rangle=g_f^{-1}\epsilon+O(\epsilon^2)\ . \tag{2.28}$$

Thus, the Lorenz truncation incorporates the correct modes of the Boussinesq equations (2.2) near threshold in the absence of modulation.

For finite modulation amplitude one could generalize the amplitude equation (2.24) to

$$\tau_0\dot{x}(t)-\tilde{\epsilon}(t)x(t)+x^3(t)=0\ , \tag{2.29}$$

where

$$\epsilon(t)\equiv\tilde{r}(t)-1\ . \tag{2.30}$$

As discussed in Sec. III, however, the threshold of (2.29) is trivial (i.e., $\epsilon_c\equiv 0$) in contrast to the behavior of the Lorenz model (2.7) or the Boussinesq equations (2.2).

D. Rigid horizontal boundaries

For the case of rigid horizontal boundaries a simple mode truncation analogous to (2.7) is still possible (see for example Gresho and Sani[17]), though the convective threshold and slope of the Nusselt number are not exact even in the absence of modulation (see below). On the other hand, an amplitude equation (2.24) can be derived near threshold, giving the correct slow time dependence and static properties in that case.[26,27,21] The only difference with the free case is that the constants τ_0 and g are now given by the values

$$\tau_0=(\tau_0^r)_{\rm ex}=(\sigma+0.5117)/19.65\sigma\ , \tag{2.31a}$$

$$(g_r)_{\rm ex}=0.6994-0.0047\sigma^{-1}+0.0083\sigma^{-2}\ , \tag{2.31b}$$

respectively. To derive the Lorenz model from a three-mode truncation of the Galerkin expansion of Gresho and Sani[17] valid for rigid boundaries, we may use the same method as described in Appendix A for the case of stress-free horizontal boundaries. The derivation will be given explicitly for gravity modulation in Sec. II E below. For a sinusoidal modulation of the temperature of the lower plate one arrives precisely at the Lorenz model of (2.7), (2.14), and (2.16) [or equivalently (2.18)–(2.23)], but with parameters

$$\tau_1=\tau_1^r=(2\pi^2)^{-1}\ , \tag{2.32a}$$

$$\tilde{\sigma}=\tilde{\sigma}_r=27\sigma/14\ , \tag{2.32b}$$

$$b=b_r=2\ , \tag{2.32c}$$

$$g=g_r=\tfrac{3}{5}\ , \tag{2.32d}$$

$$\tilde{\Delta}(\omega)=\tilde{\Delta}_r(\omega)=\Delta\left[\frac{9\pi^4\gamma}{2\tan(\gamma/2)(\pi^2-\gamma)(9\pi^2-\gamma)}\right]\ , \tag{2.32e}$$

$$\gamma=(i\omega)^{1/2}\ . \tag{2.32f}$$

The critical parameters of the three-mode truncation[17] are $k_c=0.987\pi=3.101$ and $R_c^{\rm stat}=0.999\,76\pi^6243/128=1824.7$, in contrast to the exact values[21] $k_c=3.117$ and $R_c^{\rm stat}=1707.8$. For numerical convenience we have used $k_c=\pi$ and $R_c^{\rm stat}=\pi^6243/128=1825.1$.

The amplitude equation resulting from this rigid truncation has the form (2.24) with $g=g_r$ given by (2.32d), and

$$\tau_0=\tau_0^r=(1+\tilde{\sigma}_r)\tau_1^r/\tilde{\sigma}_r=(\sigma+0.52)/2\pi^2\sigma\ . \tag{2.32g}$$

Comparing Eqs. (2.31a) and (2.32g) we see that the damping constant $\tau_0=m\Gamma$ of Eq. (2.18) is given to excellent approximation by the Lorenz truncation. The approximate coupling constant g_r in Eq. (2.32d) differs by about 15% from the exact value (2.31b), except for very small Prandtl numbers ($\sigma<0.1$) for which the difference becomes significant.[28]

E. Gravity modulation

Instead of varying the force which drives the convection by modulating the temperature difference across the cell one can also vary the buoyancy force by modulating the gravity restoring force. In this subsection we therefore consider constant temperatures at the top and bottom plates but vary the Rayleigh number $r(t)/r_0=g(t)/g$ by oscillating the cell up and down with an acceleration $g(t)$ around the gravitational acceleration $g=\langle g(t)\rangle$. Here $r_0=\langle r(t)\rangle$ denotes as before the mean reduced Rayleigh number. Again we decompose the temperature field $T(\mathbf{x},t)$ into the conducting profile (which is here linear and time independent) and the deviation $\theta(\mathbf{x},t)$ due to convection. The standard Lorenz truncation of the Boussinesq equations in terms of one velocity mode, $x(t)$, and two temperature modes, $y(t)$ and $z(t)$, then leads to the system

$$\tau_1\frac{d}{dt}x(t)=-\tilde{\sigma}x(t)+\tilde{\sigma}r(t)y(t)/r_0\ , \tag{2.33a}$$

$$\tau_1\frac{d}{dt}y(t)=-y(t)+[r_0-z(t)]x(t)\ , \tag{2.33b}$$

$$\tau_1\frac{d}{dt}z(t)=-b[z(t)-x(t)y(t)]\ , \tag{2.33c}$$

with τ_1, b, and $\tilde{\sigma}$ given by Eqs. (2.8) and (2.9) for stress-free boundaries. Again the time-dependent driving is parametric; however, since gravity modulation affects primarily the buoyancy, the parametric forcing appears in the momentum balance equation (2.2a) and hence in the first equation of the Lorenz model, (2.33a). Temperature modulation, on the other hand, affects primarily the heat balance (2.2b) thus entering the Lorenz model via the equation for y.

Linearizing (2.33) around the conductive state $x=y=z=0$, one obtains (see also Gresho and Sani[17])

$$m\ddot{y}+m\Gamma\dot{y}-[r(t)-1]y=0\ . \tag{2.34}$$

Hence the threshold for onset of convection would be the same as for the temperature modulation (2.18)–(2.21) were it not for the difference between $\tilde{r}(t)$, (2.10), and $r(t)$, (2.11). This difference, being caused by the additional driving due to the deviation S^∞ [Eq. (2.10)] of the conductive temperature profile from linearity, vanishes only in the limit $\omega\to 0$ [see Eq. (A8)]. Thus for very slow modulation $\tilde{r}(t)\to r(t)$, and the two driving mechanisms have the same thresholds for onset of convection (see Secs. III C and III F). On the other hand, the behavior above threshold is different for the two driving mechanisms even if one were to ignore the difference between $\tilde{r}(t)$ and $r(t)$. For example, the mechanical analogue of Eq. (2.33) involves the variable y and is quite different from (2.18) (see Sec. IV).

It is interesting to compare Eq. (2.33) with the systematic analysis of Davis,[20] valid near threshold in the limit $\sigma\to\infty$. To carry out the comparison we write Eq. (5.1) of Davis

$$\dot{Y}-\gamma_0(t)Y+\gamma_2(t)Y^3=0\ , \tag{2.35a}$$

$$\gamma_0=\tfrac{3}{2}[\epsilon-r_0g(t)]=\tfrac{3}{2}[r(t)-1]\ , \tag{2.35b}$$

$$\gamma_2=\tfrac{9}{8}J_2^{-1}(t)J_3(t)r(t)\ , \tag{2.35c}$$

$$\dot{J}_3(t)=r(t)J_2(t)\ , \tag{2.35d}$$

$$J_2(t)=\exp\left[t+3\int_0^t r(t')dt'\right]\equiv\exp[J_4(t)]\ , \tag{2.35e}$$

where we have used Eq. (4.2) of Davis,[20] and noted that $d=\pi$ and $\tau_1^f=\frac{2}{3}$ in his units. We now let $y=(\sqrt{3}/4)Y$, so that (2.35a) becomes

$$\tau_1^f\dot{y}(t)-[r(t)-1]y(t)+\gamma(t)r(t)y^3(t)=0\ , \tag{2.36a}$$

$$\gamma(t)=4J_3(t)J_2^{-1}(t)\ , \tag{2.36b}$$

$$\tau_1^f\dot{\gamma}(t)=\tfrac{8}{3}\{r(t)-\tfrac{1}{4}[1+3r(t)]\gamma(t)\}\ . \tag{2.36c}$$

The convective current at the bottom plate may be calculated using Eq. (A27) of Appendix A below and Eqs. (3.3d), (4.6a), (4.6c), (4.2b), and (5.1b) of Davis,

$$j^{\rm conv}(t)=-r_0A^2(t)\frac{\partial}{\partial x_3}T_2(x_3,t)\,|_{x_3=0}$$
$$=\tfrac{3}{2}r_0G_1^2(t)A^2(t)J_2^{-1}(t)J_3(t)=2r_0y^2(t)\gamma(t)\ . \tag{2.37}$$

Turning to the Lorenz model (2.33) in the limit $\sigma\to\infty$, we have

$$x(t)=[r(t)/r_0]y(t)\ , \tag{2.38}$$

and setting

$$j^{\rm conv}(t)=2z(t)\equiv 2r_0y^2(t)\gamma(t)\ , \tag{2.39}$$

Eq. (2.33) reduces to (2.36a) with

$$\tau_1^f\dot{\gamma}(t)=\tfrac{8}{3}\{r(t)-\tfrac{1}{4}[1+3r(t)]\gamma(t)\}$$
$$+2r(t)[\gamma^2(t)y^2(t)+\tfrac{4}{3}(1-r_0^2)/r_0^2]\ . \tag{2.40}$$

The difference between Eqs. (2.36) and (2.37) above derived by Davis,[20] and the Lorenz-model result (2.40) obtained in the limit $\sigma\to\infty$, is in the last term in (2.40), which only contributes to $j^{\rm conv}(t)$ at order y^4 or $y^2(r_0-1)$. We therefore see that in the order at which the analysis of Davis[20] is systematic near threshold (i.e., order y^2 in $j^{\rm conv}$), it agrees with the Lorenz model, thus providing an additional justification for the latter.

As mentioned above, for gravity modulation Gresho and Sani[17] have treated the case of rigid horizontal boundaries using a Galerkin expansion scheme. The lowest-order truncation is given by retaining only the $i=1$ modes in their Eqs. (4), (5), and (7)–(10),

$$\dot{T}_1=-(\pi^2+\alpha^2)T_1+2\sqrt{R}B_{11}V_1-2A_{111}V_1\overline{T}_1\ , \tag{2.41a}$$

$$\dot{V}_1=-(\sigma/C_{11})\{D_{11}V_1+\alpha^2\sqrt{R}\,[1+\Delta\cos(\omega t)]B_{11}T_1\}\ , \tag{2.41b}$$

$$\dot{\bar{T}}_1=-4\pi^2\bar{T}_1+A_{111}V_1T_1\ , \tag{2.41c}$$

$$j^{\rm conv}=(N-1)R/R_c=(2\pi\sqrt{R}/R_c)\bar{T}_1\ , \tag{2.41d}$$

where we have changed i^2 to $(2i)^2$ in the linear term on the rhs of their Eq. (8), in agreement with their Eq. (19), and we have replaced their $\epsilon\sin(\omega t)$ by our $\Delta\cos(\omega t)$. We may evaluate the constants B_{11}, D_{11}, C_{11}, and A_{111} from the formulas in the Appendix of Gresho and Sani[17] and we find $B_{11}=-4/3\pi$, $D_{11}=-27\pi^4/8$, $C_{11}=-7\pi^2/8$, and $A_{111}=-\frac{8}{5}$, with a wave vector $\alpha\simeq\pi$ for which $R_c^{\rm stat}\simeq 243\pi^6/128$. (Note that the expression for D_{ij} in the last equation of the Appendix of Gresho and Sani[17] is incorrect, though the integral expression given earlier is correct and yields our value.) Let us set $V_1=(5\pi^2/4)x$, $T_1=-(5R_c^{\rm stat}/3\pi\sqrt{R})y$, $\bar{T}_1=(5R_c^{\rm stat}/6\pi\sqrt{R})z$, and $r(t)=r_0[1+\Delta\cos(\omega t)]$, $r_0=R/R_c^{\rm stat}$. Then Eqs. (2.41) become precisely Eqs. (2.33) and (2.16) above, with parameter values given by Eqs. (2.32a)—(2.32d).

III. CONVECTIVE THRESHOLD: DAMPED OSCILLATOR WITH PARAMETRIC MODULATION

At the convective threshold of the Lorenz model the conductive solution $x=y=z=0$ becomes unstable against infinitesimal perturbations. The stability boundary is given by a hyperplane in parameter space at which the solution of (2.7) or (2.18) when linearized around the origin, i.e., of

$$m\ddot{x}+m\Gamma\dot{x}-\tilde{\epsilon}(t)x=0\ , \tag{3.1a}$$

$$\tilde{\epsilon}(t)=\tilde{r}(t)-1\ , \tag{3.1b}$$

is marginally stable. Beyond the stability boundary the solution of (3.1) diverges, but the nonlinearities of (2.7) provide growth limits. According to Floquet theory of linear differential equations with periodically varying coefficients,[19] the trivial solution $x=0$ of (3.1) bifurcates in a Hopf bifurcation, harmonically into a periodic orbit $x(t)=x(t+\tau)$ with the same period τ as the modulation, or subharmonically such that $x(t)=-x(t+\tau)=x(t+2\tau)$ has twice the periodicity of the driving. Note that in the subharmonic case $x(t)$ (i.e., the direction of the fluid's motion in the rolls) has to change sign.

A. Stability thresholds for harmonic and subharmonic bifurcations

We have studied the stability boundaries of the $x=0$ solution of Eq. (3.1) quantitatively for modulations

$$\tilde{\epsilon}(t)=\epsilon+\tilde{\delta}\,c(\omega t) \tag{3.2}$$

with a cosine (damped Mathieu equation) modulation

$$c(\omega t)=\cos(\omega t)\ , \tag{3.3}$$

or a step modulation

$$c(\omega t)=\begin{cases}1 & \text{for } 0<\omega t\le\pi\\ -1 & \text{for } \pi<\omega t\le 2\pi,\end{cases} \tag{3.4}$$

around a mean

$$\epsilon=r_0-1=\langle r(t)\rangle-1=\langle\tilde{r}(t)\rangle-1 \tag{3.5}$$

(see Appendix B). We shall first treat the case of (2.12)—(2.15) of a sinusoidal *temperature* modulation,

$$r(t)=r_0+\delta\cos(\omega t)\ , \tag{3.6a}$$

with a real amplitude

$$\delta=r_0\,|\,\Delta\,|\ . \tag{3.6b}$$

Then according to (2.14)

$$\tilde{r}(t)=r_0+\tilde{\delta}\cos(\omega t)\ , \tag{3.6c}$$

$$\tilde{\delta}=r_0\,|\,\tilde{\Delta}(\omega)\,|\ , \tag{3.6d}$$

with $\tilde{\Delta}(\omega)$ given by Eq. (2.15) or (2.32e) for stress-free and rigid boundaries, respectively. In the case of *gravity* modulation discussed in Sec. III F below, only $r(t)$ enters Eqs. (2.33), so $\tilde{\delta}$ is replaced by δ in Eq. (3.2). In Fig. 1 we show the threshold $\epsilon_c(\tilde{\delta},\omega)$ for harmonic and subharmonic bifurcations as a function of $\tilde{\delta}$ for cosine as well as step modulation, and representative values of ω and σ ($\omega=13.32$, $\sigma=1$, $\Gamma/\omega=2.222$). These curves were obtained numerically as described in Appendix B. There we also include the stability charts for several other values of the normalized damping Γ/ω in the parameter range of interest to our problem.

For small $\tilde{\delta}$ the bifurcation is harmonic. Only with larger modulation amplitudes can one drive the system into a subharmonic orbit (in the case treated in Fig. 1, for

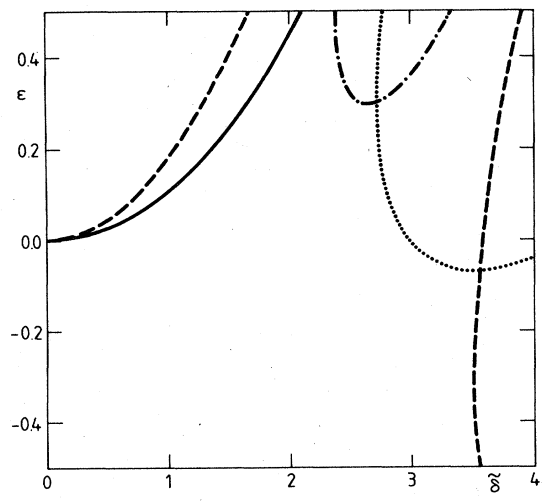

FIG. 1. Linear stability boundaries of the trivial solution $x=0$ of (3.1) as a function of modulation amplitude $\tilde{\delta}$, Eq. (3.6), for $\sigma=1$, $\omega=13.32$ ($m=1.14\times10^{-3}$, $\Gamma/\omega=2.222$). Solid and dashed lines denote harmonic bifurcation thresholds for cosine [Eq. (3.3)] and step [Eq. (3.4)] modulations, respectively. Dotted and dash-dotted lines represent the corresponding stability boundaries for subharmonic Hopf bifurcations, with twice the period.

$\tilde{\delta} \gtrsim 2.3$). In general there is for increasing $\tilde{\delta}$ a succession of harmonic and subharmonic instabilities (cf. Appendix B).

B. Dynamical stabilization of $x=0$ state

Note the general tendency for dynamical stabilization[17,19] of the $x=0$ state by modulation with small amplitude, $\epsilon_c(\tilde{\delta},\omega) > \epsilon_c(\tilde{\delta}=0)=0$. This feature cannot be reproduced by the standard amplitude equation with periodically modulated coefficients since Eq. (3.1) without the second-order time derivative [e.g., Eq. (2.29)] has $\epsilon_c=0$. This result may be derived simply by dividing the amplitude equation (2.29) by x and averaging over a period. One thus obtains the relation

$$\langle x^2(t)\rangle = \epsilon \ , \tag{3.7}$$

which implies $\epsilon_c=0$. The physical reason for the lack of stabilization in the amplitude equation is the absence of inertia, an effect which enhances the basin of attraction of the $x=0$ fixed point for small $\tilde{\delta}$. Indeed, rolling downwards from the origin during those times where the potential of (3.1) is curved downwards [$\tilde{r}(t)>1$] is delayed by inertia (the particle spends more time in the vicinity of $x=0$). Thus in a symmetric modulation around $\epsilon=0$ the particle moves closer inwards during the times when $\tilde{r}(t)<1$ than it moves outwards when $\tilde{r}(t)>1$. Consequently the stabilization is most pronounced for large modulation periods, i.e., the second-derivative term in (3.1) becomes more important than the first-derivative rather than less important as $\omega \to 0$. Note, however, that the above discussion excludes all additional forces, e.g., fluctuations or other inhomogeneities, which drive the system away from its fixed point $x=0$ (cf. Sec. V below).

For large modulation amplitudes the situation is more complicated. There stabilization, $\epsilon_c>0$, as well as destabilization, $\epsilon_c<0$, occur depending on the sizes of r_0, $\tilde{\delta}$, and ω (cf. Fig. 1 and Appendix B).

C. Low-frequency limit

For low frequencies $\tilde{\delta}$ is replaced by δ [cf. Eq. (3.6)], and the threshold $\epsilon_c(\delta, \omega \to 0)$ of the Lorenz model coincides for arbitrary δ with that of the Boussinesq equations with free boundary conditions as evaluated by Rosenblat and Herbert[7] and by Dowden.[15] The basic physical reason is that $x(t)$, the $n_3=1$ Fourier mode of the vertical velocity field, is the first one to grow; when it becomes marginally stable the others are still damped as noted by Rosenblat and Herbert.[7] Moreover, these authors show that the threshold $\epsilon_c(\delta, \omega \to 0)$ is determined solely by the $n_3=1$ mode (higher velocity modes $n_3>1$ do not enter) and that the critical wave number is $\pi/\sqrt{2}$ as for static driving.

In fact the starting equation (2.15) of Rosenblat and Herbert[7] for the $n_3=1$ modes reduces exactly to our Eq. (3.1) if the coupling constants P_{1m} to modes $m>1$, which do not enter anyhow, are set equal to zero. The correspondence between the paper of Rosenblat and Herbert[7] and our work is demonstrated by observing that $\epsilon \leftrightarrow \Delta = \delta/r_0$, $\lambda_1(\sigma+1) \leftrightarrow \Gamma$, $\sigma\lambda_1^2 \leftrightarrow 1/m$, $R\sigma a^2/\lambda_1 \leftrightarrow r/m$, and $P_{11}e^{it}+\tilde{P}_{11}e^{-it} \leftrightarrow \mathrm{Re}[\tilde{\Delta}(\omega)e^{-it}]$.

For the sake of completeness we give the formula [Eq. (4.12) of Rosenblat and Herbert[7]] which determines the zero-frequency threshold $\epsilon_c = r_c - 1$:

$$\left[\frac{\Gamma}{2}\right]^2 = \left[\frac{\delta+\epsilon_c}{m}+\frac{\Gamma^2}{4}\right]\left[\frac{2E(k)}{\pi}\right]^2 , \tag{3.8a}$$

where $E(k)$ is the complete elliptic integral of the second kind[29] with

$$\frac{k^2}{2} = \frac{\delta}{\delta+\epsilon_c+m\Gamma^2/4} \ . \tag{3.8b}$$

For graphs of $\epsilon_c(\delta,\sigma,\omega=0)$ we refer to Figs. 1 and 2 of Rosenblat and Herbert.[7]

The modes with $n_3>1$ enter into the low-frequency correction to the threshold of the full Boussinesq equations. However, since the correction $\phi(\delta)$ defined by

$$r_c(\delta,\omega)/r_c(\delta,\omega=0) = 1+\omega^2\phi(\delta) \tag{3.9}$$

was found[7] to be very small, generally of the order of 10^{-2}, we expect the Lorenz model to give a reasonable approximation for finite frequencies also.

Rosenblat and Herbert obtained the above results with a WKB expansion which restricts the size of the modulation amplitude, e.g, $\delta < r_0$ for $\sigma=1$. Subsequently Dowden[15] extended this analysis to arbitrary δ. Since the deviation $S^\infty(x_3,t)$ (cf. Appendix A) of the conductive temperature profile from a linear one vanishes for $\omega \to 0$ Dowden ignored S^∞ from the beginning. In that case different Fourier modes of the fields decouple in the linearized Boussinesq equations. It follows that for the $n_3=1$ velocity mode with (critical) wave number $\sqrt{\pi}/2$ the Boussinesq equations reduce exactly to the linearized Lorenz model (3.1) with $\tilde{r}(t)$ replaced by $r(t)$, i.e., $\tilde{\delta}(\omega)$ replaced by $\delta=\tilde{\delta}(\omega=0)$ [cf. Eq. (6) of Dowden; for direct comparison, note that his times are scaled by d^2/ν while ours are measured in units of d^2/κ]. Dowden's stability relations obtained from asymptotic solutions of the Mathieu equations for $\omega \to 0$ confirm and extend the previous result of Rosenblat and Herbert. Again the least stable mode is $n_3=1$ and $\sqrt{\pi}/2$ is the critical wave number so that the threshold may be obtained from Eq. (3.1).

D. Small modulation amplitude

Here we present an analytic expression for the harmonic bifurcation threshold $\epsilon_c(\tilde{\delta},\omega)$ at small $\tilde{\delta}$ (i.e., $\tilde{\delta} \ll 1$) but arbitrary ω, and compare the Lorenz model result with the linear stability analysis[16] of the Boussinesq equations.

1. Bifurcation threshold of the modulated oscillator

In Appendix B we expand $\epsilon_c(\tilde{\delta},\omega)$ as well as the periodic orbit $x(t)$ at threshold in powers of $\tilde{\delta}$, and seek at each order the marginally stable periodic solution of (3.1) and (3.2). We obtain up to quadratic order in $\tilde{\delta}$

$$\epsilon_c(\tilde{\delta},\omega) = \frac{\tilde{\delta}^2}{m\Gamma^2} \begin{cases} \dfrac{1}{2}\dfrac{1}{1+(\omega/\Gamma)^2}, & \text{cosine modulation} \qquad (3.10a) \\ 1-\dfrac{\tanh(\pi\Gamma/2\omega)}{\pi\Gamma/2\omega}, & \text{step modulation} \ . \qquad (3.10b) \end{cases}$$

As noted already, the dynamic stabilization of the $x=0$ state induced by small-amplitude modulation is largest for small ω, and it decreases monotonically to zero with increasing ω. We may also note that for $\omega\to 0$ Eq. (3.10a) yields $\epsilon_c=\delta^2/2m\Gamma^2$, which agrees with the small-δ expansion of (3.8). For a light particle ($m\to 0$) moving with finite friction ($m\Gamma$ finite) the effect of dynamical stabilization [(3.10a) and (3.10b)] vanishes linearly with m: $\epsilon_c\sim m$. The threshold shift at low frequencies $\epsilon_c(\tilde{\delta},\omega\to 0)/\tilde{\delta}^2$ for a step is twice as big as for a cosine modulation. The "effective," mean-square modulation amplitude of the latter is only one-half that of the former.

2. *Convective threshold of the Lorenz model*

For sinusoidal temperature modulations (2.12) we obtain in the Lorenz model from (3.10a) and (3.6c)

$$\epsilon_c^L(\delta,\omega)=\epsilon_c^L(\delta,\omega=0)[1+\omega^2\tau_1^2/(\tilde{\sigma}+1)^2]^{-1}\,|\,\tilde{\Delta}(\omega)/\Delta\,|^2\,, \tag{3.11a}$$

$$\epsilon_c^L(\delta,\omega=0)=\delta^2\frac{\tilde{\sigma}/2}{(\tilde{\sigma}+1)^2}\,, \tag{3.11b}$$

as a function of the modulation amplitude $\delta=r_0\,|\,\Delta\,|$. In the above formulas we used Eqs. (2.19) and (2.20) and we may insert the corresponding values of τ_1, $\tilde{\sigma}$, and $\tilde{\Delta}$ for free and rigid cases, respectively. It is intersting to note that at low frequencies the shift (3.11) of the convective threshold is largest for $\tilde{\sigma}=1$, in which case the prefactor in (3.11b) is $\frac{1}{8}$; this occurs for Prandtl numbers $\sigma=1$ in the free case and $\sigma\simeq\frac{1}{2}$ in the rigid case [see Eqs. (2.8b) and (2.32b)].

3. *Convective threshold of the Boussinesq equations: stress-free boundaries*

Venezian[16] has determined the convective threshold of the full Boussinesq equations for small-amplitude sinusoidal temperature modulation in a laterally infinite system with stress-free boundary conditions at the top and bottom plates. He considered three cases.

(i) Modulation of the temperature of the lower plate only:

$$T^l(t)=T^u+R\ \mathrm{Re}(1+\Delta e^{-i\omega t})\,. \tag{3.12a}$$

(ii) Out-of-phase modulation of top and bottom plate:

$$T^{u\atop l}(t)=T_0\mp\tfrac{1}{2}R\ \mathrm{Re}(1+\Delta e^{-i\omega t})\,. \tag{3.12b}$$

(iii) In-phase modulation of top and bottom plate:

$$T^l(t)=T^u(t)+R=T_0+\tfrac{1}{2}R\ \mathrm{Re}(1+\Delta_V e^{-i\omega t})\,, \tag{3.12c}$$

with amplitude Δ_V. Note that for modulation (iii) the temperature difference between bottom and top plate is constant in time, $R(t)=R$.

In all three cases the threshold shifts turn out to be given by a sum of contributions $K(n_3,\omega)$ from the various field amplitudes, $n_3=1,2,\ldots$, arising in the Fourier decomposition with respect to the vertical coordinate x_3. To make the comparison we write

$$\epsilon_c^V(\delta_V,\omega)=\epsilon_c^L(\delta,\omega)+\delta_V^2\sum_{n_3=2}^{\infty}K(n_3,\omega)\,. \tag{3.13}$$

with

$$\delta_V=\begin{cases}\delta=r_0\,|\,\Delta\,|\,, & \text{for (i),(ii)} \quad (3.14)\\ r_0\,|\,\Delta_V\,|\,, & \text{for (iii)}\,. \quad (3.15)\end{cases}$$

The $n_3=1$ term

$$\delta^2K(n_3=1,\omega)=\epsilon_c^L(\delta,\omega) \tag{3.16}$$

gives just the threshold (3.10a) of the Lorenz model.

In all three cases (3.12) the higher modes, $n_3\geq 2$, do not contribute to the low-frequency threshold shift since $K(n_3\geq 2,\omega\to 0)=0$, so the Lorenz model reproduces the exact low-frequency convective threshold (cf. Sec. III C). For the in-phase modulation (iii) $\delta=0$ and hence $\epsilon_c^L=0$ for all frequencies whereas (3.13) is finite due to contributions from higher modes. However, the threshold shift by in-phase modulation is small for all values of σ (cf. dots in Fig. 2). In cases (i) and (ii) the Lorenz-model contribution is dominant at small σ. With increasing σ the $n_3\geq 2$ contributions gain relative weight, but then the total size of the threshold shift decreases as well. Figure 2 shows

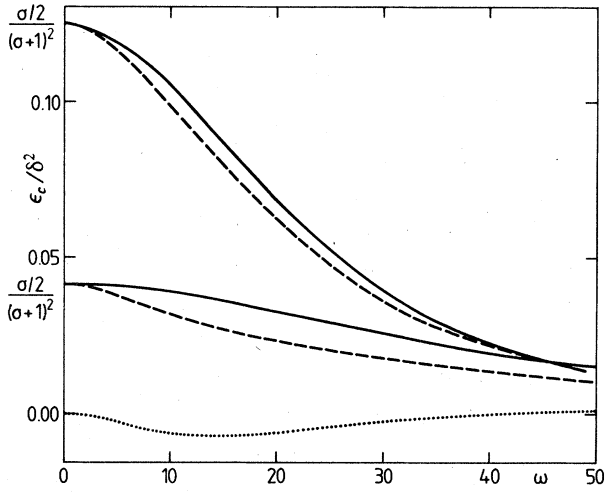

FIG. 2. Frequency dependence of ϵ_c/δ^2 where ϵ_c is the convective threshold shift and δ is the modulation amplitude defined in Eq. (3.6a). Upper and (lower) solid curve denotes ϵ_c/δ^2 obtained within the Lorenz model for $\sigma=1$ ($\sigma=10$) for (i) bottom heating only and (ii) out-of-phase modulation of top and bottom plate. In the Lorenz model (i) and (ii) yield the same threshold. Upper dashed curve is the result obtained by Venezian (Ref. 16) for the full Boussinesq equations with stress-free boundaries expanded to second order in δ for case (i) of bottom heating and $\sigma=1$ (the lower dashed curve is for $\sigma=10$). Venezian's thresholds ϵ_c/δ_V^2 for case (ii) are identical within the resolution of the figure to the Lorenz-model curves. Dots denote the threshold shift ϵ_c/δ_V^2 of the Boussinesq equations (Ref. 16) for case (iii) of an in-phase temperature modulation of both plates, such that the temperature difference is time independent, $\delta\equiv 0$. For this type of modulation the Lorenz model yields $\epsilon_c\equiv 0$.

the good agreement of the Lorenz-model result with Venezian's expression $\epsilon_c^V(\delta,\omega)/\delta^2$ for the convective threshold of the full Boussinesq equations, for Prandtl numbers $\sigma=1$ and 10 and modulation according to (i) and (ii). In fact for case (ii) Venezian's result is identical within the resolution of Fig. 2 to the Lorenz-model threshold.

E. Convective threshold for rigid boundaries

As mentioned in Sec. II, for this case we still use Eqs. (2.7), (2.14), and (2.16) but with parameters given in Eq. (2.32). The linear problem is then still given by (3.1), with

$$m=m_r=\tilde{\sigma}_r^{-1}(\tau_1^r)^2=(\sigma\pi^4 54/7)^{-1}\ , \tag{3.17}$$

$$\Gamma=\Gamma_r=(\tilde{\sigma}+1)/\tau_1^r=2\pi^2(1+27\sigma/14)\ . \tag{3.18}$$

The threshold for the full Boussinesq equations with rigid velocity boundary conditions has been evaluated numerically by Rosenblat and Tanaka[18] using a Galerkin expansion. In Fig. 3 we show some of the results of their calculation as open circles, and those obtained from the Lorenz model as described in Appendix B as a solid line, for the case $\Delta=0.4$ and $\sigma=1$. Although there is no expansion in the amplitude $\delta=r_0\Delta$ in the present case, we still use the same representation as in Fig. 2, in terms of ϵ_c/δ^2, since it magnifies differences at small δ (even so, the discrepancies are insignificant). Similar results are also obtained for $\Delta=1$. In Fig. 4 we plot the threshold shift as a function of σ, at fixed $\Delta=1$ and $\omega=1$, and find once again excellent agreement between our model and the numerical work of Rosenblat and Tanaka. Note also that the results for rigid boundaries do not differ much from those for free boundaries shown in Figs. 1 and 2, once the threshold is normalized by its value $R_c^{\rm stat}$ in the absence of modulation.

F. Convective threshold for gravity modulation

Since for gravity modulation the conductive temperature profile is linear in x_3 it does not introduce additional

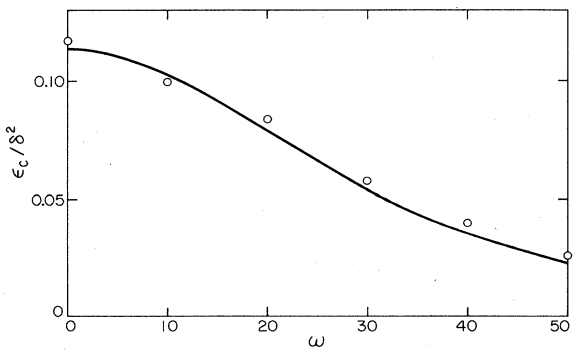

FIG. 3. Convective threshold ϵ_c/δ^2 for rigid horizontal boundaries as a function of ω for a relative modulation amplitude $\Delta=0.4$ and Prandtl number $\sigma=1$. Solid line denotes the Lorenz-model stability boundary for rigid boundaries. Circles represent the result obtained from a Galerkin expansion of the full Boussinesq equations; the values have been read as well as possible from Fig. 1 of Ref. 18.

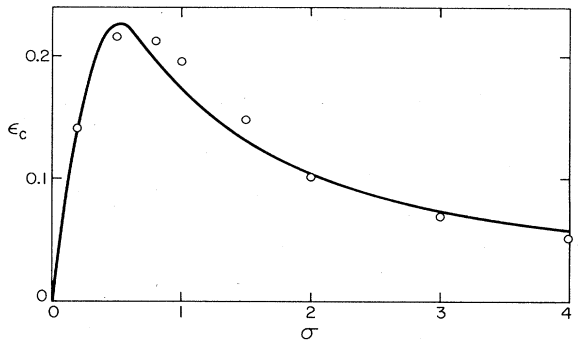

FIG. 4. Convective threshold ϵ_c for rigid horizontal boundaries as a function of Prandtl number σ, for fixed frequency $\omega=1$ and relative modulation amplitude $\Delta=1$. Solid line denotes the Lorenz model (as in Fig. 3) and the circles represent the numerical calculation of Rosenblat and Tanaka, obtained from Fig. 5 of Ref. 18.

spatial dependence into the linearized Boussinesq equations

$$[(\partial_t-\nabla^2)(\partial_t-\sigma\nabla^2)\nabla^2-\sigma R(t)(\nabla_1^2+\nabla_2^2)]u_3(\mathbf{x},t)=0\ . \tag{3.19}$$

In contrast to temperature modulation, different Fourier modes in the vertical ($\hat{\mathbf{x}}_3$) direction are linearly decoupled and each has its own threshold determined by a Mathieu equation with parameters depending on n_3 and the lateral wave number. For the mode $n_3=1$ which grows first, one obtains for the critical wave number $\sqrt{\pi}/2$, Eq. (2.34), with the same values of m and Γ as in the Lorenz model, Eqs. (2.19) and (2.20). Hence the linearized Lorenz model (2.34) reproduces the convective threshold of the Boussinesq equations for arbitrary sinusoidal gravity modulation and stress-free horizontal boundaries. For small amplitude the result is

$$\epsilon_c(\omega,\delta)=\delta^2\frac{\tilde{\sigma}/2}{(\tilde{\sigma}+1)^2}\left[1+\left[\frac{\omega\tau_1}{\tilde{\sigma}+1}\right]^2\right]^{-1}\ , \tag{3.20}$$

which differs from the corresponding result for temperature modulation, Eq. (3.11), due to the difference between $r(t)$, Eq. (2.12), and $\bar{r}(t)$, Eq. (2.14).

IV. NONLINEAR BEHAVIOR IN THE PRESENCE OF MODULATION

In this section we discuss the effect of the nonlinearities of our model on its behavior near threshold.

A. Analytic theories

The nonlinear behavior of the modulated Lorenz model is rather difficult to study analytically, even near threshold, but we have found numerically that the memory term $M[x]$ in (2.18) does not contribute significantly in the parameter region of interest ($r_0\lesssim 2$, $|\Delta|\lesssim 1$). It is therefore useful to study first the simpler case $M\equiv 0$ and then the full Lorenz model.

1. Anharmonic oscillator and amplitude equation

Setting $M\equiv 0$ in Eq. (2.18) one obtains the parametrically modulated anharmonic oscillator

$$m\ddot{x}+m\Gamma\dot{x}=[\epsilon+\tilde{\delta}\cos(\omega t)]x-x^3\equiv\tilde{\epsilon}x-x^3 . \quad (4.1)$$

This model was discussed by Davis and Rosenblat[19] and by Lücke and Schank;[30] the present discussion gives additional motivation for investigating (4.1) in the fluid-dynamical context.

Near the (shifted) threshold $x(t)$ is small and we can attempt to calculate it analytically using perturbation theory. The expansion parameter is the square root of the distance $\epsilon-\epsilon_c(\tilde{\delta},\omega)$ from the shifted threshold discussed in Sec. III. This expansion was discussed by Davis and Rosenblat,[19] who pointed out that the coefficients diverge as $\omega\to 0$ at fixed $\tilde{\delta}$, in which case the problem is inherently nonlinear and no analytic expression is known. Their argument is repeated in Appendix C, where it is argued, however, that the range of validity of perturbation theory is in fact larger than stated by Davis and Rosenblat, though their basic point, that perturbation theory breaks down for ω sufficiently small, is still valid. Indeed, the whole discussion can also be applied to the simpler generalized amplitude equation

$$\dot{x}-[\epsilon+\tilde{\delta}\cos(\omega t)]x+x^3=0 , \quad (4.2)$$

which follows from (4.1) in the limit $m\to 0$, $m\Gamma\to 1$. For (4.2) the exact solution is known, and again one finds that perturbation theory fails for $\omega\to 0$ at fixed $\tilde{\delta}$ (for this case $\epsilon_c\equiv 0$). Both Eqs. (4.1) and (4.2) are discussed in Appendix C where it is shown that near threshold there are two regimes:

(i) Perturbative regime: $\epsilon-\epsilon_c\ll 1$, $\epsilon<\tilde{\delta}$, $\epsilon-\epsilon_c\ll\omega$, but $\omega/\tilde{\delta}$ arbitrary. In this region the perturbation theory of Davis and Rosenblat[19] is valid, even when $\omega/\tilde{\delta}\ll 1$, so long as $\epsilon-\epsilon_c\ll\omega$. In particular, it is not necessary that the condition $\omega/\tilde{\delta}\gtrsim 1$ be satisfied, contrary to the statement of Davis and Rosenblat. Our evidence for this assertion is the exact solution of the amplitude equation (4.2), and a numerical solution of the nonlinear oscillator model which agrees rather well with the perturbative result for $\epsilon-\epsilon_c\ll\omega\ll\tilde{\delta}$ (see Appendix C).

(ii) Nonperturbative regime: $\epsilon-\epsilon_c\ll 1$, $\epsilon<\tilde{\delta}$, $\omega\ll\epsilon-\epsilon_c$. In this region the solutions are not expandable in powers of $\epsilon-\epsilon_c$, and the problem is essentially nonlinear as stressed by Davis and Rosenblat.[19] We have not found the analytic form of the solution of Eq. (4.1) in this regime, and even for the amplitude equation the exact solution is rather complicated.

There is another parameter range where an analytic solution is possible, namely the *adiabatic* regime, at low frequencies and above threshold.

(iii) Adiabatic regime: $\omega\ll\tilde{\delta}<\epsilon$. In this case

$$\tilde{\epsilon}(t)\equiv\epsilon+\tilde{\delta}\cos(\omega t) \quad (4.3)$$

never falls below its threshold value in the absence of modulation [$\tilde{\epsilon}(t)=0$], and the solutions may be systematically expanded at low frequencies around the quasistatic solution of (4.1), or (4.2),

$$x_{qs}(t)=[\tilde{\epsilon}(t)]^{1/2} , \quad (4.4)$$

with corrections of relative order $\omega/\tilde{\epsilon}$ (see Appendix C).

It is interesting to note that the adiabatic expansion makes no specific reference to the particular form used for $\tilde{\epsilon}(t)$, so long as it has period $2\pi/\omega$ and average ϵ. In particular, for any $\tilde{\epsilon}$ we show that for $\omega\to 0$ we must have

$$\epsilon_c(\tilde{\delta},\omega\to 0)<\tilde{\delta} , \quad (4.5)$$

since otherwise we could choose $\tilde{\delta}<\epsilon<\epsilon_c$ and be below threshold ($\langle x^2\rangle=0$), in violation of (4.4). The case of a step-function modulation has the advantage that the linear problem can be solved analytically (see Appendix B), but the nonlinear analysis is somewhat simpler for the cosine modulation.

In the perturbative regime (i) the expansion coefficients of $x(t)$ can be evaluated from the solutions of the linear equation (3.1). These solutions can be obtained analytically within a small-$\tilde{\delta}$ expansion as shown in Appendix C. The resulting average convective current is expressed in the form

$$g\langle j^{\rm conv}(t)\rangle=\langle x^2(t)\rangle=[\epsilon-\epsilon_c(\tilde{\delta},\omega)]s(\tilde{\delta},\omega)+O((\epsilon-\epsilon_c)^2) , \quad (4.6a)$$

$$s(\tilde{\delta},\omega)=1-\tilde{\delta}^2 s^{(2)}(\omega)+O(\tilde{\delta}^4) , \quad (4.6b)$$

with ϵ_c given by Eq. (3.10a) to $O(\tilde{\delta}^2)$. The calculation of Appendix C yields

$$s^{(2)}(\omega)=\frac{2}{m^2}\frac{1}{(\omega^2+\Gamma^2)^2}=\frac{2\tilde{\sigma}^2}{(\tilde{\sigma}+1)^4}\left[\frac{1}{1+\omega^2\tau_1^2/(\tilde{\sigma}+1)^2}\right]^2 . \quad (4.7)$$

To compare the above results (4.6) and (4.7) for the anharmonic oscillator [$M=0$ in (2.18)] with those of the Lorenz model ($M\neq 0$) one has to use the fact that according to (3.6) $\tilde{\delta}=|\tilde{\Delta}(\omega)/\Delta|\,\delta$ for a sinusoidal temperature modulation $r(t)=r_0+\delta\cos(\omega t)$ with real amplitude $\delta=r_0|\Delta|$.

2. Lorenz model

Let us now consider the full Lorenz model for a sinusoidal temperature modulation (2.7) and for a sinusoidal gravity modulation (2.33). The average convective current is given by an equation analogous to (4.6),

$$g\langle j^{\rm conv}(t)\rangle=\langle z(t)\rangle=[\epsilon-\epsilon_c(\delta,\omega)]s(\delta,\omega)+O((\epsilon-\epsilon_c)^2) , \quad (4.8a)$$

$$s(\delta,\omega)=1-\delta^2 s^{(2)}(\omega)+O(\delta^4) , \quad (4.8b)$$

with coefficients calculated in Appendix C to be

$$s_T^{(2)}(\omega)=\frac{\tilde{\sigma}}{b(\tilde{\sigma}+1)^4}[b(\tilde{\sigma}-1)+2\tilde{\sigma}(\tilde{\sigma}+1)+(\omega\tau_1)^2]\,|\,\tilde{\Delta}(\omega)/\Delta\,|^2[1+\omega^2\tau_1^2/(\tilde{\sigma}+1)^2]^{-2}(1+\omega^2\tau_1^2/b^2)^{-1}\,, \tag{4.9}$$

$$s_G^{(2)}(\omega)=\frac{\tilde{\sigma}}{2b(\tilde{\sigma}+1)^4}\{b(\tilde{\sigma}-1)(\tilde{\sigma}^2+2\tilde{\sigma}+3)-2(\tilde{\sigma}+1)(\tilde{\sigma}^2+1)+[(\tilde{\sigma}-1)(b+\tilde{\sigma}-1)-\tilde{\sigma}^2-1](\omega\tau_1)^2\}$$
$$\times[1+\omega^2\tau_1^2/(\tilde{\sigma}+1)^2]^{-2}(1+\omega^2\tau_1^2/b^2)^{-1}-\tilde{\sigma}(\tilde{\sigma}+1)^{-2}[1+\omega^2\tau_1^2/(\tilde{\sigma}+1)^2]^{-1}\,, \tag{4.10}$$

where the subscripts T and G denote temperature and gravity modulation respectively, and the corresponding threshold shifts are given by (3.11) and (3.20). The coefficients b, $\tilde{\sigma}$, τ_1, and $|\tilde{\Delta}(\omega)/\Delta|$ in the above equations are given in Eqs. (2.8), (2.9), and (2.15) for free boundaries and in Eq. (2.32) for rigid boundaries.

If we take the limit $\tilde{\sigma}\to\infty$ in Eqs. (4.9) and (4.10) we find $s_T^{(2)}\to 0$, whereas $s_G^{(2)}$ remains finite. These results may be obtained directly from the starting equations by noting that for $\tilde{\sigma}\to\infty$ Eqs. (2.7) reduce to

$$\tau_1\dot{y}=(\tilde{r}-1)y-zy\,, \tag{4.11a}$$

$$\tau_1\dot{z}=-b(z-y^2)\,, \tag{4.11b}$$

whereas Eqs. (2.33) yield

$$\tau_1\dot{y}=(r-1)y-rzy/r_0\,, \tag{4.12a}$$

$$\tau_1\dot{z}=-b(z-ry^2/r_0)\,. \tag{4.12b}$$

Thus for temperature modulation

$$\tau_1\langle\dot{y}/y\rangle=\langle\tilde{r}-1-z\rangle=0=\epsilon-\langle z\rangle\,, \tag{4.13a}$$

and

$$s_T\equiv 1,\quad s_T^{(2)}=0\,. \tag{4.13b}$$

For gravity modulation, on the other hand,

$$\langle z\rangle=\langle ry^2\rangle/r_0\neq\epsilon\,, \tag{4.14a}$$

and in general

$$s_G\neq 1,\quad s_G^{(2)}\neq 0\,, \tag{4.14b}$$

[cf. Eqs. (2.39) and (2.40)].

B. Numerical study

The full Lorenz model (2.7) may be simply integrated numerically in order to check the various results and assertions of the analytic study. In addition, the comparison with experiment to be carried out in paper II will be based entirely on the numerical results. In this section we present some results of integrations of the Lorenz model for rigid boundaries, given by Eqs. (2.7), (2.12)–(2.14), and (2.16) with parameters (2.32a)–(2.32c) and (2.33e) (we need not specify the value of g_r in these calculations). In the case of gravity modulation Eq. (2.7) is replaced by (2.33) with

$$r(t)=r_0 g(t)/g=r_0\mathrm{Re}(1+\Delta e^{-i\omega t})\,. \tag{4.15}$$

The average convective current is given by

$$\langle j^{\mathrm{conv}}(t)\rangle=g_r^{-1}\langle z(t)\rangle \tag{4.16}$$

and $\langle z(t)\rangle$ was calculated as a function of the average reduced Rayleigh number $\epsilon=r_0-1$, for various values of Δ, ω, and σ. The threshold ϵ_c at which a finite $\langle j^{\mathrm{conv}}\rangle$ first appears is analogous to that shown in Fig. 1, where a subharmonic bifurcation is found above a certain value of Δ. In the present calculations we chose $\omega=6$, $\sigma=1$ as an example, and found subharmonic bifurcations for $\Delta>\Delta_2$ with $\Delta_2=1.21$ for temperature modulation and $\Delta_2=1.19$ for gravity modulation. The variation of $\langle j^{\mathrm{conv}}\rangle$ with ϵ is shown in Fig. 5(a) for temperature modulation with various fixed values of Δ. For $\Delta\gtrsim\Delta_2$ the convective current seems to grow discontinuously as ϵ crosses the threshold, i.e., the subharmonic bifurcation appears to be inverted. For $\Delta<\Delta_2$, on the other hand, the current grows linearly with $\epsilon-\epsilon_c$ (the harmonic bifurcation is supercritical). The normalized slope at fixed Δ

$$S\equiv g_r\frac{d}{d\epsilon}\langle j^{\mathrm{conv}}\rangle\Big|_{\epsilon=\epsilon_c}\equiv\frac{d\langle z\rangle}{d\epsilon}\Big|_{\epsilon=\epsilon_c} \tag{4.17}$$

resulting from Fig. 5(a) is plotted in Fig. 5(b), as a function of Δ (solid curve). This slope becomes very small just below Δ_2, and it is strictly speaking undefined for $\Delta\gtrsim\Delta_2$. For $\Delta\gtrsim 1.3$, however, Fig. 5(a) indicates that an effective slope can be obtained from the data. This slope is also shown in Fig. 5(b). The model has also been solved for the case of gravity modulation. The corresponding slopes are shown by the dashed curve of Fig. 5(b), which shows significant differences with the case of temperature modulation. The dependence of the slope S on ω and σ is illustrated in Figs. (5c) and (5d) for both temperature and gravity modulation, and once again it shows interesting differences between the two.

The above initial slope S of $\langle z(t)\rangle$ [Eq. (4.17)] is obtained for fixed Δ. To compare with the analytical results (4.8)–(4.10) one has to take into account that $\delta=(1+\epsilon)|\Delta|$ depends on ϵ, so that

$$S(\Delta,\omega)=s(\delta_c,\omega)+\frac{\delta_c}{1+\epsilon_c}\frac{\partial\langle z(t)\rangle}{\partial\delta}\Big|_{\epsilon=\epsilon_c,\ \delta=\delta_c}\,, \tag{4.18}$$

with $\delta_c=(1+\epsilon_c)|\Delta|$. To second order in Δ one obtains

$$S(\Delta,\omega)=1-|\Delta|^2[s^{(2)}(\omega)+2\epsilon_c^{(2)}(\omega)]+O(\Delta^4)\,, \tag{4.19}$$

where $s^{(2)}(\omega)$ is given by (4.9) or (4.10) and $\epsilon_c^{(2)}(\omega)$ is the second-order coefficient of the threshold shift. We have compared the small-Δ numerical calculation with the analytically evaluated slope $S(\Delta,\omega)$ in (4.19), and the agreement is excellent as indicated in Fig. 5(b).

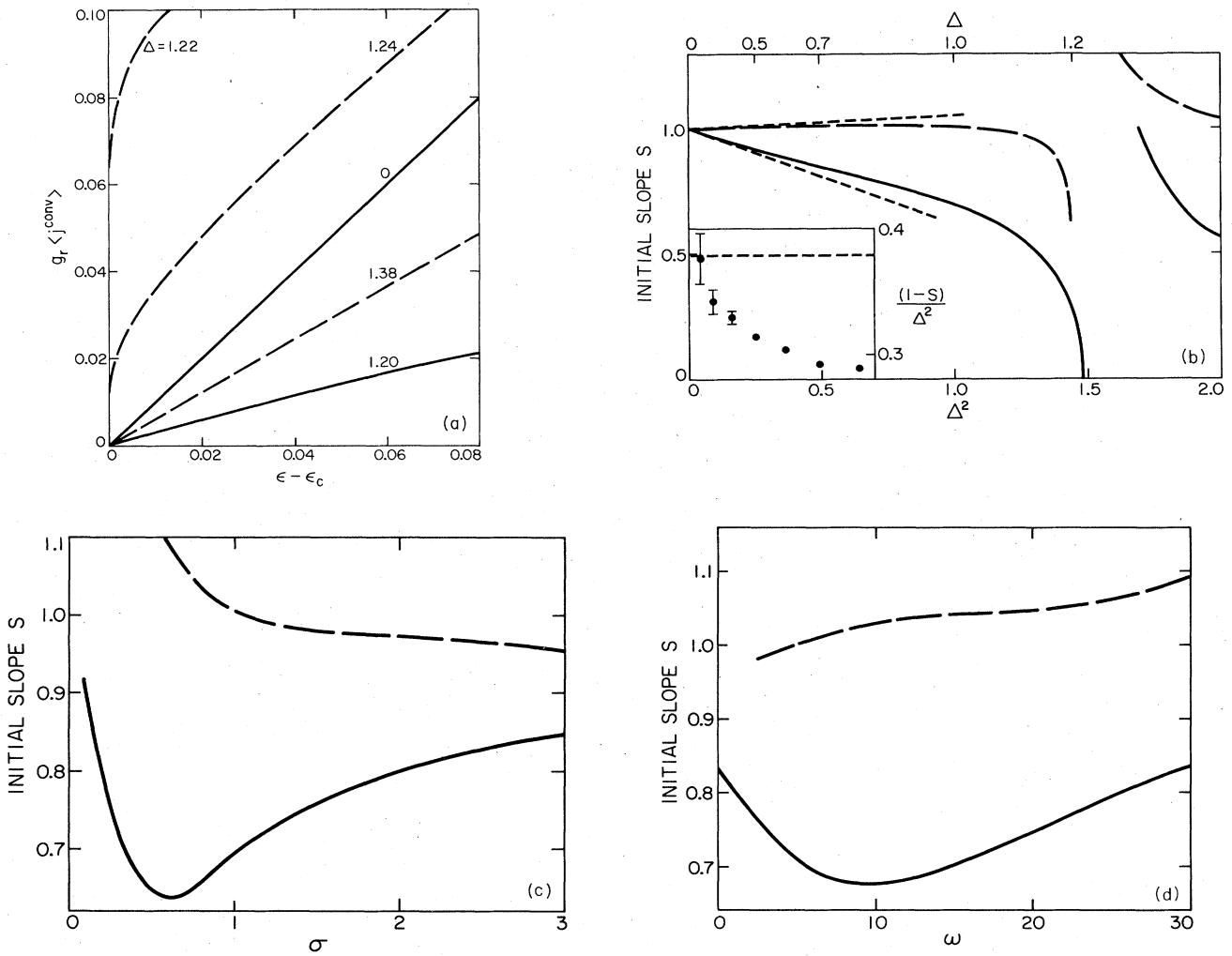

FIG. 5. (a) Average convective current $\langle j^{conv}\rangle$ vs average reduced Rayleigh number $\epsilon-\epsilon_c$ for temperature modulation at fixed frequency $\omega=6$, Prandtl number $\sigma=1$, and for different values of the relative modulation amplitude Δ. The harmonic bifurcation for $\Delta<\Delta_2=1.21$ (solid lines) is supercritical. The subharmonic bifurcation for $\Delta\gtrsim\Delta_2$ (dashed lines) appears to be subcritical. The scale of the ordinate, $g_r\langle j^{conv}\rangle=\langle z\rangle$, is chosen so that in the absence of modulation ($\Delta=0$, $\epsilon_c=0$) the slope is unity ($\langle z\rangle=\epsilon$). (b) Slope $S=g_r d\langle j^{conv}\rangle/d\epsilon\,|_{\epsilon=\epsilon_c}=d\langle z\rangle/d\epsilon\,|_{\epsilon=\epsilon_c}$ plotted vs Δ (upper scale) or Δ^2 (lower scale). The solid line, which is obtained from data similar to those in (a), is for temperature modulation, and the long-dashed line is for gravity modulation with the same ω and σ. The corresponding small-Δ analytic results of Eqs. (4.9), (4.10), and (4.19) are shown as short-dashed lines. Inset in the lower left-hand corner shows on a more sensitive scale the consistency at small Δ between the analytic and numerical results for temperature modulation, by plotting $(S-1)/\Delta^2$ vs Δ^2. Error bars indicate the accuracy of our numerical results (solid circles), and the dashed horizontal line is the analytic value. (c) Initial slope S plotted vs Prandtl number for fixed $\omega=6$ and $\Delta=1$, for temperature modulation (solid line) and gravity modulation (dashed line). (d) Same plot as in (c) except vs frequency ω for fixed $\sigma=1$.

The foregoing results are definite predictions of the model which would be interesting to test experimentally. Some of these tests do not appear easy to perform, however, for the following reasons. First, gravity modulation seems difficult to realize experimentally with amplitudes bigger than $\Delta=10^{-2}$, say, so the interesting behavior is not attainable in that case. Second, as discussed in Sec. V below, the threshold behavior in real systems is significantly perturbed by imperfections, the most important one coming from sidewall heating. Thus the nonlinear behavior of most real systems differs appreciably from that of the ideal model studied in this section. It is possible, nevertheless, that future experiments might be designed to minimize sidewall effects, in which case some of the nonlinear features of the model displayed here might be realized. In general, however, it is important to take the sidewalls effects into account in the theory in order to obtain realistic predictions which permit comparison with experiment. This we have done in Sec. V below and in paper II.

C. Comparison with previous authors

We have already seen that for the case of gravity modulation the Lorenz model (2.33) agrees with the amplitude

equation of Davis,[20] Eq. (2.36) above, valid for $\sigma\to\infty$, up to terms of order y^5. Thus, the behavior near threshold, and in particular the slope $s(\delta,\omega)$ of Eq. (4.8), will be identical.

Finucane and Kelly[5] have also studied a truncated nonlinear model, which they obtained from "energy relations." The results were then compared to experiment and to other analytic results (termed "periodicity theory") which come from the linearized Boussinesq equation. In fact, it appears to us that the difference between their "periodicity" theory [Eq. (4.8) of Ref. 5] and their "energy" theory [Eqs. (4.25), (4.26), and (4.29)] is primarily that between a linear and a nonlinear theory, but both approaches should yield essentially the same threshold behavior. Indeed, from their definitions (4.24), the modes A, B, and C of Finucane and Kelly are seen to be proportional to our x, y, and z, respectively. With the identifications $a^2=\pi^2/2$, $x=A/(2\pi\sqrt{3})$, $y=Br_0\pi\sqrt{3}/4$, and $z=-Cr_0\pi$, Eqs. (4.25), (4.26), and (4.29) of Finucane and Kelly become

$$\tau_1^f\dot{x}=-\sigma(x-y)\ , \tag{4.20a}$$

$$\tau_1^f\dot{y}=-y+[r(t)-z]x\ , \tag{4.20b}$$

$$\tau_1^f\dot{z}=-\tfrac{8}{3}(z-xy)\ , \tag{4.20c}$$

i.e., the Lorenz model (2.7) with parameters appropriate to free boundaries, except that $\tilde{r}(t)$ is approximated by $r(t)$ (linear conduction profile). Note that the stability domain of the conductive state, $x=y=z=0$, is enhanced, $r_c(\Delta,\omega)>1$, by small-amplitude modulation at low frequencies irrespective whether $\tilde{r}(t)$ or $r(t)$ is used in (4.20b) (cf., Appendix B). Hence the dashed theoretical curves in Figs. 21 and 22 of Finucane and Kelly,[5] showing "onset of observable motion" for values of $r_0<1$, must refer entirely to *transient* behavior. The transient convective current predicted by (4.20) for $r_0<1$ depends sensitively on the initial values chosen for the variables x,y,z. For short times those play a role analogous to our forcing function ξ (see Sec. V), but the initial values disappear from the theory at long times where the ideal behavior is recovered. Presumably, their experiments could be analyzed in terms of our Eq. (5.2) below, in which the system reaches a steady state independent of initial values [see also the discussion below Eq. (26) of Gresho and Sani[17]].

V. EFFECT OF SIDEWALLS: IMPERFECT BIFURCATION

In this section we investigate the effect of lateral walls at $x_1=\pm L$ for a system with stress-free horizontal boundaries. The system is still taken to be infinite in the x_2 direction.

A. Derivation of the forcing term

As mentioned in the Introduction, Cross *et al.*[22] studied the effect of time-dependent sidewall heating on the amplitude equation, and found a forcing term given in Eq. (1.7), whose strength agreed in order of magnitude with the one inferred from the experiments on convective onset times by Ahlers *et al.*[21] The forcing field ξ, when added to the amplitude equation (1.6), excites a convection pattern $x(t)=\hat{u}_1(1,0,1)$ of rolls parallel to the x_2 axis, i.e., parallel to the sidewall. This correctly reproduces the experimental fact that the heat current caused by the dynamic mismatch between the sidewall and the fluid has a strong dependence on the coordinate x_1 perpendicular to the sidewall, and depends only weakly on the coordinate x_2. For time-independent heating, on the other hand, and for sidewalls which are thermally clamped to the top and bottom plates, there is no such forcing term and we expect rolls perpendicular to the sidewalls to be favored, at least over a large portion of the cell. The applicability of our theory thus depends on the forcing term (1.7) being sufficiently strong to suppress these perpendicular rolls. Although we do not at present have an *a priori* theoretical estimate for the strength of the required forcing, there is recent experimental evidence[13] that modulation indeed leads to concentric rolls in a cylindrical container, in agreement with our assumption.

In order to adapt the calculation of Cross *et al.*[22] to our model we shall repeat their derivation, but retain only the three modes x,y,z of the original model. For consistency we shall therefore assume *periodic* velocity boundary conditions at the sidewalls $\mathbf{u}(x_1=-L,x_2,x_3)=\mathbf{u}(x_1=L,x_2,x_3)$ so that the previously defined Fourier modes of $\mathbf{u}$ are still appropriate. The change in thermal boundary condition leads to an additional (wall) contribution $S_w(x_1,x_3,t)$ to the conducting temperature profile in the fluid (see Appendix D)

$$T^{\rm cond}(\mathbf{x},t)=R(t)(1-x_3)+S^\infty(x_3,t)+S_w(x_1,x_3,t)\ , \tag{5.1}$$

where $S^\infty(x_3,t)$ is the deviation from a linear profile in the laterally infinite system [Eq. (A4)]. We may now insert (5.1) into the Boussinesq equations (2.2) and once again project out the three Lorenz modes x,y,z. For stress-free horizontal boundaries we then find (see Appendix D) that the Fourier modes $\hat{S}_w(n_1,0,n_3;t)$ of the wall contribution modify the Lorenz equations additively as well as multiplicatively. The most important effect (and the only one we shall retain) is a change of Eq. (2.7a) to

$$\tau_1\dot{x}(t)=-\tilde{\sigma}[x(t)-y(t)]+\tilde{\sigma}\xi(t)\ , \tag{5.2}$$

where $\xi(t)$ has the same periodicity as the drive $\tilde{r}(t)$. Its Fourier coefficients are given by

$$\xi_\nu=-i\omega\nu f\left[\frac{T_\nu^l+T_\nu^u}{R_c^{\rm stat}}\right]\psi(\omega\nu)\ , \tag{5.3}$$

where $\psi(\omega\nu)$ is a complicated but smooth function given in Eq. (D18) and satisfying $\psi(0)=1$, $\psi\to0$ for $\omega\nu\to\infty$. The constant[31] f,

$$f=-\frac{\sqrt{2}(1-\lambda_1)\cos\alpha}{\pi^3L[1+\lambda_2\coth(\pi t_w)]}\ , \tag{5.4a}$$

is determined by the ratios

$$\lambda_1=\kappa_f/\kappa_w,\quad \lambda_2=K_f/K_w\ , \tag{5.4b}$$

of thermal diffusivities and conductivities of the fluid and wall materials, respectively, the dimensionless wall thickness t_w, the lateral width of the layer $2L$ (the limit

$\pi L \gg 1$ is assumed), and the phase angle

$$\alpha=\pi L/\sqrt{2}-\cot^{-1}(\sqrt{2})\ . \tag{5.4c}$$

An interesting property of Eq. (5.3) is that ξ vanishes for antisymmetric heating of the upper and lower plates ($T_v^l=-T_v^u$), a result which does not depend on the truncation, but only on the Boussinesq approximation (2.2). In addition, f vanishes for $\lambda_1=1$, or $\lambda_2\to\infty$, or $L\to\infty$, since there is no lateral heat flow in those cases. For bottom-plate modulation only, the function ξ is proportional to the time derivative $\dot{r}(t)$, and an expression similar to that of Cross *et al.*[22] is recovered. The differences lie in the value of the constant f, and in the function $\psi(\omega\nu)$ which was set equal to unity by Cross *et al.* since the calculation was for low frequencies.

It must be noted that our detailed expression for f is not to be taken too seriously since the mode truncation we use is a particularly poor approximation near the sidewall. Indeed, the temperature profile $S_w(x_1,x_3,t)$ is sufficiently large to couple effectively to many velocity modes and thus to generate velocity field excitations which are localized near the sidewalls. Within our truncation scheme, however, these modes which are not excited in the bulk are discarded, and we therefore examine only the effect of S_w on the velocity mode $x=\hat{u}_1(1,0,1)$, Eq. (5.2). Moreover, we have not attempted to repeat the calculation of Appendix D for rigid boundaries. In comparing our theory with experiments we shall treat the constant f as an adjustable parameter, which is either fixed to agree with the theoretical value calculated by Cross *et al.*[22] at low frequencies, or taken from the experimental value obtained by Ahlers *et al.*[21] in the absence of modulation. Alternatively, we can adjust f to fit modulation experiments at one particular frequency and amplitude, and then examine the frequency and amplitude dependence of the data.[11,3] These various adjustments of the single constant f involve relatively small changes about a common value which gives semiquantitative agreement with experiment.

B. Effects of the forcing: imperfect bifurcation

The behavior of the model of (2.7) and (2.32a)—(2.32c) with (2.7a) replaced by

$$\tau_1^r\frac{dx}{dt}=-\sigma[x(t)-y(t)]+\sigma\xi(t)\ , \tag{5.5}$$

and ξ given in Eq. (5.3), is illustrated in Fig. 6 for various values of the constant f and constant values of σ, ω, and $\delta=r_0\Delta$. It is seen that the bifurcation at threshold goes from being perfect for $\xi=0$ (dot-dashed curve) to imperfect for $\xi\neq 0$ (solid and dashed curves). This means that there is no uniquely defined threshold for convection, though one can introduce an apparent threshold $\epsilon_c^{\rm eff}(z_0)$, defined as the value of ϵ at which the normalized convective current $\langle z\rangle=g_r\langle j^{\rm conv}\rangle$ reaches the value z_0 [the ideal threshold is $\epsilon_c=\epsilon_c^{\rm eff}(z_0=0)$]. In Fig. 7 we plot the apparent thresholds $\epsilon_c^{\rm eff}(z_0=10^{-2})$ and $\epsilon_c^{\rm eff}(z_0=10^{-3})$ as a function of frequency for fixed δ and σ and various values of ξ (or f). It is seen that although the forcing ξ becomes small at low frequencies [cf. Eq. (5.3)] it has a large effect

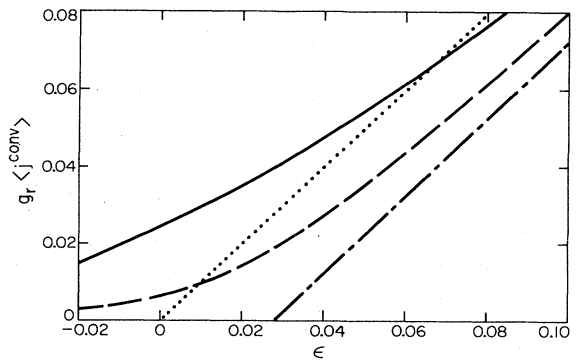

FIG. 6. Average normalized convective current $g_r\langle j^{\rm conv}\rangle$ plotted vs average reduced Rayleigh number ϵ, in the presence of the forcing field ξ [Eqs. (5.3)—(5.5)], and fixed modulation amplitude $\delta=r_0\Delta=0.5$, frequency $\omega=6$, and Prandtl number $\sigma=1$. Solid curve is for a typical experimental forcing strength $f=4.0\times10^{-3}$, the dashed curve is for $f=1.3\times10^{-3}$, the dot-dashed curve is the ideal case $f=0$, while the dotted curve is the unmodulated result ($\delta=0$).

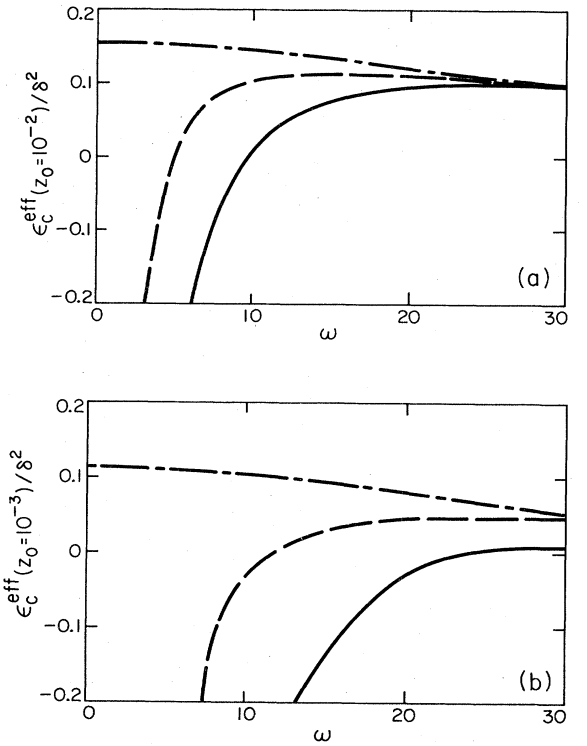

FIG. 7. Effective threshold $\epsilon_c^{\rm eff}(z_0)$ (defined as the reduced Rayleigh number ϵ at which $\langle z\rangle=g_r\langle j^{\rm conv}\rangle$ reaches the value z_0) plotted as a function of frequency ω for various values of the forcing parameter f, and fixed modulation amplitude $\delta=0.5$ and Prandtl number $\sigma=1$. Curves correspond to the same f values as in Fig. 6, namely, solid curve, $f=4.0\times10^{-3}$; dashed curve, $f=1.3\times10^{-3}$; dot-dashed curve, $f=0$. (a) is $\epsilon_c^{\rm eff}$ ($z_0=10^{-2}$) and (b) is $\epsilon_c^{\rm eff}$ ($z_0=10^{-3}$). The ideal curve $\epsilon_c=\epsilon_c^{\rm eff}z_0=0$ for $f=0$ is indistinguishable from the dot-dashed curve in (b).

on the apparent threshold. This is because the convective current remains above a minimum value set by ξ during the subcritical part of each period, so that it has enough time to build up to a macroscopic value during the supercritical part of the period. Figure 7 bears a certain resemblance to Fig. 1 of Davis,[4] which summarizes the different criteria used to define stability of time-dependent motion in the presence of fluctuations. Our parametrization of the problem in terms of a forcing field ξ seems to us to be a physically appropriate description, even in cases where the detailed theory we have developed for ξ is inapplicable.

C. Transitions induced by the forcing

The Lorenz-model equations (2.7), as well as the anharmonic oscillator (4.1) have a symmetry $x \leftrightarrow -x$, so that each solution is doubly degenerate. This degeneracy is lifted by the forcing ξ, and it is interesting to consider transitions from one orbit to the other induced by ξ. For a *qualitative* discussion let us consider the oscillator model

$$m\ddot{x}+m\Gamma\dot{x}-[\epsilon+\delta\cos(\omega t)]x+x^3=\xi(t) \tag{5.6}$$

with

$$\xi(t)=-f\omega\delta\sin(\omega t)=f\dot{r}(t)\ , \tag{5.7}$$

which is a good approximation to the Lorenz model at low frequencies. In the absence of modulation ($\delta=0$), the degenerate fixed points are $x_\pm=\pm\epsilon^{1/2}$ for $\epsilon>0$, and a constant forcing $\xi_0>0$ would favor the fixed point x_+. Nevertheless, the fixed point x_- still has a sizeable basin of attraction, so ξ_0 would have to be larger than some finite threshold [which depends on ϵ and the initial value $x(0)$] in order to cause a transition from x_- to x_+.

In the modulated case it turns out that a very small forcing can already cause a transition from the $x<0$ orbit to the $x>0$ orbit. This is because the oscillator can come very close to $x=0$ at some time during its period, at which point the restoring force $\partial U/\partial x=-[\epsilon+\delta\cos(\omega t)]x+x^3$ is very small. Let us consider a low-frequency situation ($\omega/\Gamma\ll 1$), when our classical particle moves quasiadiabatically with the potential U. Then the points of closest approach to $x=0$ are near the increasing zeros of the drive, $\omega t^*\simeq 3n\pi/2$ (n an integer), since immediately before t^* the potential is upward ($\partial^2U/\partial x^2>0$), while immediately after it is downward ($\partial^2U/\partial x^2<0$). At $\omega t=3n\pi/2$ the forcing ξ is maximal (cf. the dash-dotted curve in Fig. 8) and the restoring force minimal, so the former has its largest effect. If the phase of ξ is such that $\xi(t^*)>0$, a crossing from the $x_-(t)$ to the $x_+(t)$ orbit is favored, say, whereas if $\xi(t^*)<0$, such a crossing is prevented. If for given parameter values the forcing is too small to cause crossing, then its critical value can be reached by either of the following procedures: (i) increasing f or δ, (ii) decreasing ϵ, and (iii) decreasing ω. Obviously (i) directly increases the forcing while (ii) decreases the Rayleigh number and with it the convective amplitude x so that $x_{\min}$ comes closer to zero. Procedure (iii) is more subtle. While decreasing ω also decreases ξ there is the countereffect of decreasing the distance $\epsilon-\epsilon_c(\delta,\omega)$ from the ideal threshold, thus causing the amplitude $|x_{\min}|$ to become smaller.

Figure 8 demonstrates how a critical forcing is reached by increasing δ. There the thick lines represent $x(t)$ obtained from integrating the Lorenz model, Eqs. (5.2), (2.7b), and (2.7c), numerically for $\sigma=1$, $\tau_1^f=2/3\pi^2$, $\epsilon=r_0-1=0.1$, and $\omega=3$ ($\omega/\Gamma=0.1$), with a forcing given by Eq. (5.7) with $f=0.005$. The dashed thin lines show the time variation of the external driving $r(t)-1$ and the thin dash-dotted lines represent $30\xi(t)$. In the upper part of Fig. 8 the relative modulation amplitude $\Delta=\delta/r_0=0.4$ entails a forcing ξ that is too small to induce a crossing from the unfavored x_- orbit (lower thick curve in the top half of Fig. 8) to the favored x_+ orbit (upper thick curve in the top half of Fig. 8) near the times $\omega t/2\pi=n\,3/4$ marked by arrows. Thus the x_- solution is stable [Fig. 8 shows $x_\pm(t)$ after 25 driving periods have elapsed since starting the system from $x_0=y_0=\pm 0.3962$, $z_0=0.157$]. In the lower part of Fig. 8 ($\Delta=0.5$) the forcing is sufficiently strong to induce a crossing from x_- to x_+.

In a measurement one does not necessarily observe $x(t)$ directly but rather $x^2(t)$. However, this quantity also depends on the occurrence of a crossing. First, note that just below the critical forcing the average over a period $\langle x_+^2(t)\rangle$ of the favored solution will be considerably larger than $\langle x_-^2(t)\rangle$ (e.g., in the top half of Fig. 8, $\langle x_+^2\rangle=2.2\langle x_-^2\rangle$). The reason is that the critical forcing

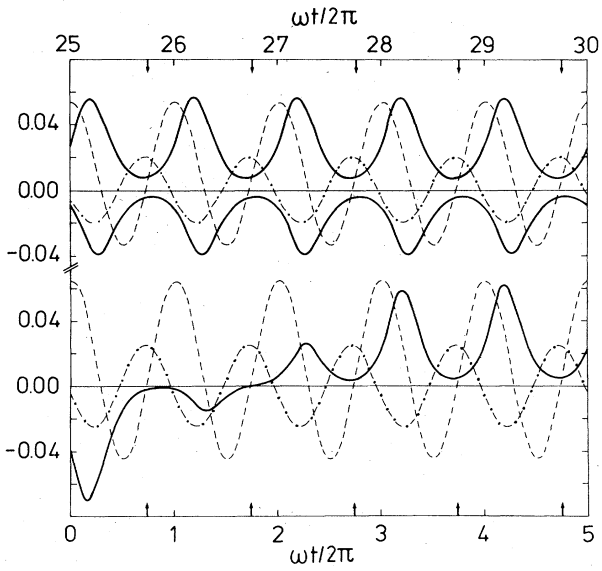

FIG. 8. Effect of time-dependent sidewall heating on the Lorenz model. Thick lines represent $x(t)$ obtained from integrating Eqs. (5.2), (2.7b), and (2.7c) numerically for $\sigma=1$, $\tau_1^f=2/3\pi^2$, $\epsilon=r_0-1=0.1$, $\omega=3$ with a wall forcing $\xi(t)=f\dot{r}(t)$ and $f=0.005$. Thin dash-dotted lines represent $30\xi(t)$. Thin dashed lines show the driving $r(t)-1$ for modulation amplitudes $\Delta=0.4$ and 0.5 in the top and bottom halves, respectively. The maxima of $\xi(t)$ at $\omega t/2\pi=3n/4$ (marked by arrows) are very close to the increasing zeros of the driving, i.e., they occur at times where the convective amplitudes are very small. The effective forcing is too weak in the top panel (but strong enough in the bottom) to induce a crossing from $x<0$ to $x>0$. See text for further details.

strongly depresses $x_-^{\min}$ at t^* thereby hindering the growth of x_- to sizable amplitudes during times where $r(t)>1$, while $x_+^{\min}$ is even enhanced by ξ at t^*. Therefore, if $x^-(t)$ is realized with a small $\langle x_-^2(t)\rangle$ for subcritical forcing, one will observe a large change in $\langle x^2(t)\rangle$ when increasing the forcing to a supercritical value (e.g., by increasing Δ), as a result of the crossing from the then unstable x_- orbit to the stable x_+ solution. The change in Fig. 8, e.g., is from $\langle x_-^2\rangle=0.4\times10^{-3}$ for $\Delta=0.4$, to $\langle x_+^2\rangle=1\times10^{-3}$ for $\Delta=0.5$. On the other hand, if x_+ is realized below the critical forcing threshold, one does not observe such a change in $\langle x^2(t)\rangle$ since the favored solution is practically unaffected by slightly increasing the forcing. For example, $\langle x_+^2(t)\rangle$ in the top and bottom of Fig. 8 differ by only 2%. Further evidence of the crossing in the Lorenz model and comparison with experiment are given in paper II.[3]

VI. CONCLUSION

Let us summarize the main results of the present work.

(1) An approximation to the Boussinesq equations was introduced to treat convection in the presence of external modulation of the temperature or gravitational force. This approximation, which consists in retaining only one velocity mode and two temperature modes, is not systematic in the sense that the errors cannot be shown to be small in any limit. On the other hand, the modes retained are treated exactly in the presence of modulation and lead to a generalization of the well known model of Lorenz, for both stress-free and rigid horizontal boundaries.

(2) A linearization of the model for temperature and gravity modulation yields the threshold shift ϵ_c for the onset of convection as a function of the amplitude and frequency of modulation. Comparison with exact calculations of ϵ_c using the linearized Boussinesq equations in certain limits yields excellent agreement wherever the threshold shift is appreciable.

(3) The nonlinear behavior of the model above threshold can be studied analytically in certain limits, and numerically for all values of the parameters. Detailed predictions are obtained for the convective current $j^{\rm conv}(t)$.

(4) An important physical effect which must be taken into account to interpret real experiments is the forcing of convection brought about by time-dependent sidewall heating. This effect is calculated exactly for stress-free horizontal boundaries within our mode truncation, and yields an imperfect bifurcation from conduction to convection. The dependence of the sidewall forcing on experimental parameters is investigated in detail. An interesting effect of the forcing is to cause a transition from one direction of flow to another as the amplitude of the modulation is increased at fixed average Rayleigh number.

In a subsequent paper[3] the foregoing theory is applied to quantitative experiments in which the heat current entering the bottom plate of a cylindrical cell was sinusoidally modulated and the temperature difference between the two plates was measured as a function of time.

Let us conclude by listing possible extensions of the theory.

(1) Clearly, to improve the theory from a fundamental point of view more modes must be retained. For rigid horizontal boundaries one could demand that enough modes be kept so that the slope of the Nusselt number versus Rayleigh number be correctly given in the absence of modulation (this is already the case for stress-free horizontal boundaries in our model). More ambitiously, one could demand that enough modes be retained to describe the subcritical bifurcation to hexagons predicted by Roppo *et al.*[12] in ideal systems.

(2) In view of the importance of sidewall forcing for real modulation experiments it would be desirable to have a more accurate representation of this effect than we have used. In particular, the local nature of this forcing is lost in our model since we only retain one spatial mode of flow. An amplitude equation which involves the spatial variation of the flow was discussed by Cross *et al.*,[22] but it has only a first time derivative and therefore would show no threshold shift with modulation. A more appropriate model would have both spatial variation and higher time derivatives, but no such model has yet been derived. An interesting possibility would be to incorporate the hexagonal convection pattern for ideal systems, and to study how it is suppressed by forcing terms in the presence of sidewalls. It seems likely that these effects could be studied numerically on the basis of phenomenological models which are constructed to agree with more exact theories in various limiting cases.

ACKNOWLEDGMENTS

The authors acknowledge valuable discussions with M. C. Cross, and the support of the National Science Foundation (NSF) under Grants No. MEA-81-17241 and No. PHY-77-27084 and of North Atlantic Treaty Organization (NATO) under Grant No. 128.82. A large portion of the present work was carried out while two of us (P.C.H. and M.L.) were at the Institute for Theoretical Physics at the University of California, Santa Barbara.

APPENDIX A: GENERALIZED LORENZ MODEL FOR STRESS-FREE HORIZONTAL BOUNDARIES

Here we derive the generalized Lorenz model (2.7) from the Boussinesq equations (2.2) for a laterally infinite fluid layer with an externally imposed vertical temperature difference varying periodically in time. Let the temperatures of the upper and lower plates be general periodic functions with period $2\pi/\omega$ (not necessarily harmonic),

$$T^u(t)=\sum_{\nu=-\infty}^{\infty} T_\nu^u e^{-i\omega\nu t}, \tag{A1}$$

$$T^l(t)-T^u(t)=R(t)=\sum_{\nu=-\infty}^{\infty} R_\nu e^{-i\omega\nu t}. \tag{A2}$$

1. Conductive state

The conductive temperature profile

$$T^{\rm cond}(x_3,t)=T^u(t)+R(t)(1-x_3)+S^\infty(x_3,t) \tag{A3}$$

resulting from the boundary conditions (2.4) in the ab-

sence of convection [$\mathbf{u}(\mathbf{x},t)\equiv 0$] is also periodic with period $2\pi/\omega$. For the laterally infinite system it depends only on the vertical coordinate, albeit nonlinearly via $S^{\infty}(x_3,t)$ which is the instantaneous deviation from a linear conduction profile. Its temporal Fourier coefficients are given by

$$S_\nu^\infty(x_3)=R_\nu\left[\frac{\sin[\gamma_\nu(1-x_3)]}{\sin\gamma_\nu}-(1-x_3)\right]+T_\nu^u\left[\frac{\sin(\gamma_\nu x_3)+\sin[\gamma_\nu(1-x_3)]}{\sin\gamma_\nu}-1\right], \tag{A4a}$$

with

$$\gamma_\nu=(i\omega\nu)^{1/2}. \tag{A4b}$$

The conductive heat current at the lower plate

$$J^{\rm cond}(t)=-\frac{\partial}{\partial x_3}T^{\rm cond}(x_3,t)\,|_{x_3=0} \tag{A5}$$

in general depends on both T^u and T^l. The relation between the corresponding harmonics is

$$J_\nu^{\rm cond}=\frac{\gamma_\nu}{\tan\gamma_\nu}\left[R_\nu+T_\nu^u\left[1-\frac{1}{\cos\gamma_\nu}\right]\right]. \tag{A6}$$

In the relation for the $\nu=0$ component, i.e., the time averages,

$$\langle J^{\rm cond}(t)\rangle=\langle R(t)\rangle, \tag{A7}$$

the temperature of the upper plate does not enter. For later reference we give the $n_3=2$ Fourier components of $S_\nu^\infty(x_3)$:

$$\hat{S}_\nu^\infty(n_3=2)=-\int_0^1 dx_3 S_\nu^\infty(x_3)\sin(2\pi x_3)=\frac{R_\nu}{2\pi}\frac{\gamma_\nu}{\gamma_\nu^2-4\pi^2}. \tag{A8}$$

2. Derivation of the Lorenz model

As described in Sec. II we decompose the temperature field into conducting and convecting parts

$$T(\mathbf{x},t)=T^{\rm cond}(x_3,t)+\theta(\mathbf{x},t). \tag{A9}$$

We then make a spatial Fourier series expansion of the velocity fields $u_j(\mathbf{x},t)$ and of the deviation $S^{\infty}(x_3,t)+\theta(\mathbf{x},t)$ from the linear conduction profile, according to

$$\phi(\mathbf{x})=i\sum_{\mathbf{n}}\hat{\phi}(\mathbf{n})e^{i\mathbf{q}(\mathbf{n})\cdot\mathbf{x}}. \tag{A10}$$

By symmetry we may choose real modes satisfying

$$\hat{\phi}(\mathbf{n})=-\hat{\phi}(-\mathbf{n}), \tag{A11}$$

with

$$\mathbf{n}=(n_1,n_2,n_3),\quad n_i=0,\pm1,\pm2,\ldots \tag{A12}$$

$$\mathbf{q}(\mathbf{n})=(k_1n_1,k_2n_2,k_3n_3),\quad k_3=\pi. \tag{A13}$$

The boundary conditions for the temperature fields

$$S^{\infty}(x_3)=\theta(\mathbf{x})=0\ \text{ at } x_3=0,1 \tag{A14}$$

imply that $\hat{S}^{\infty}(n_3)$ and $\hat{\theta}(\mathbf{n})$ are odd under $n_3\to-n_3$. The stress-free boundary condition of the velocity fields,

$$\frac{\partial u_1(\mathbf{x})}{\partial x_3}=\frac{\partial u_2(\mathbf{x})}{\partial x_3}=0\ \text{ at } x_3=0,1 \tag{A15}$$

implies that the velocity modes $\hat{u}_{1,2}(\mathbf{n})$ are even under $n_3\to-n_3$. Due to the incompressibility constraint $q_i\hat{u}_i(\mathbf{n})=0$, the vertical component $\hat{u}_3$ can be expressed in terms of $\hat{u}_{1,2}$,

$$\hat{u}_3(\mathbf{n})=-\frac{k_1n_1\hat{u}_1(\mathbf{n})+k_2n_2\hat{u}_2(\mathbf{n})}{\pi n_3}. \tag{A16}$$

Furthermore, the conductive temperature $T_{\rm cond}$ drops out of the momentum balance (2.2a) of the Boussinesq equations for the solenoidal velocity field, upon applying the transversal projector $P_{ij}=\delta_{ij}-q_iq_j/q^2$ to $\delta_{j,3}\hat{T}_{\rm cond}(n_3)$. Finally, the pressure is given by a quadratic combination of velocity components. Discarding all Fourier modes other than $\hat{u}_1(1,0,1)$ (corresponding to straight rolls along the x_1 direction) and $\hat{\theta}(1,0,1),\hat{\theta}(0,0,2)$, the Boussinesq equations (2.2) reduce to

$$\partial_t\hat{u}_1(1,0,1)=-\sigma(k_1^2+\pi^2)\hat{u}_1(1,0,1)-\sigma[k_1\pi/(k_1^2+\pi^2)]\hat{\theta}(1,0,1), \tag{A17a}$$

$$\partial_t\hat{\theta}(1,0,1)=-(k_1^2+\pi^2)\hat{\theta}(1,0,1)-(k_1/\pi)\hat{u}_1(1,0,1)[R(t)-2\pi\hat{S}^{\infty}(2,t)-2\pi\hat{\theta}(0,0,2)], \tag{A17b}$$

$$\partial_t\hat{\theta}(0,0,2)=-4\pi^2\hat{\theta}(0,0,2)-4k_1\hat{u}_1(1,0,1)\hat{\theta}(1,0,1). \tag{A17c}$$

The fact that only the mode $\hat{S}^{\infty}(n_3=2)$ of the nonlinear conductive profile enters into (A17b) is not an additional approximation but rather a consequence of the mode truncation of u and θ. From Eq. (A8a) it is seen that this coefficient is independent of T_ν^u.

By introducing

$$x=-2^{3/2}\frac{2\pi}{b}\frac{\hat{u}_1(1,0,1)}{(R_c^{\rm stat})^{1/2}}, \tag{A18a}$$

$$y=2^{3/2}\frac{\pi}{\sqrt{b}}\frac{\hat{\theta}(1,0,1)}{R_c^{\rm stat}}, \tag{A18b}$$

$$z=2\pi\frac{\hat{\theta}(0,0,2)}{R_c^{\rm stat}}, \tag{A18c}$$

as variables, Eqs. (A17) take the form given in (2.7),

$$\tau_1^f\frac{dx}{dt}=-\sigma(x-y), \tag{A19a}$$

$$\tau_1^f\frac{dy}{dt}=-y+\left[\frac{R(t)-2\pi\hat{S}^{\infty}(2,t)}{R_c^{\rm stat}}-z\right]x, \tag{A19b}$$

$$\tau_1^f\frac{dz}{dt}=-b(z-xy). \tag{A19c}$$

Here

$$R_c^{\rm stat}=\frac{(k_1^2+\pi^2)^3}{k_1^2} \tag{A20}$$

is the critical Rayleigh number for onset of convection with wave number k_1 in the absence of modulation. Equation (A20) leads to the exact critical Rayleigh number $R_c^{\rm stat}=\pi^4 27/4$, and the correct critical wave number $k_1^c=\pi/\sqrt{2}$, for which

$$b=\frac{4\pi^2}{k_1^2+\pi^2}\rightarrow\frac{8}{3}\ , \tag{A21}$$

$$\tau_1^f=\frac{1}{k_1^2+\pi^2}\rightarrow\frac{2}{3\pi^2}\ . \tag{A22}$$

[In contrast to McLaughlin and Martin[9] we choose not to rescale the time t, but keep it in units of the vertical diffusion time, thus producing the factors τ_1^f in (A19). Furthermore, our variables x,y differ from those introduced by Lorenz[8] by a factor $1/\sqrt{b}$. In that way the relation $\langle z(t)\rangle=\langle x^2(t)\rangle$ holds exactly for the time averages.]

The quantity

$$\begin{aligned}\tilde{R}(t)&=R(t)-2\pi\hat{S}^{\infty}(n_3=2,t)\\&=\sum_{\nu=-\infty}^{\infty}R_\nu\frac{4\pi^2}{4\pi^2-i\omega\nu}e^{-i\omega\nu t}\end{aligned} \tag{A23}$$

replaces the Rayleigh number in the standard Lorenz model. For a pure harmonic modulation

$$R(t)=R_0{\rm Re}(1+\Delta e^{-i\omega t}) \tag{A24}$$

one obtains

$$\tilde{R}(t)=R_0{\rm Re}\left[1+\Delta\frac{4\pi^2}{4\pi^2-i\omega}e^{-i\omega t}\right]=R_c^{\rm stat}\tilde{r}(t)\ . \tag{A25}$$

[In the main text of the paper we have used the usual symbol R instead of R_0 for the average Rayleigh number $\langle R(t)\rangle$.] Lastly we mention that the vertical heat current averaged horizontally

$$J(x_3,t)=\langle u_3(\mathbf{x},t)T(\mathbf{x},t)\rangle_{x_1,x_2}-\frac{\partial}{\partial x_3}\langle T(\mathbf{x},t)\rangle_{x_1,x_2} \tag{A26}$$

is determined at the lower plate $x_3=0$ by the temperature only. Hence the convective contribution to the current

$$\begin{aligned}J^{\rm conv}(t)&=-\frac{\partial}{\partial x_3}\langle\theta(\mathbf{x},t)\,|_{x_3=0}\rangle_{x_1,x_2}\\&=2\pi\sum_{n_3=1}^{\infty}n_3\hat{\theta}(0,0,n_3;t)\end{aligned} \tag{A27}$$

is given in the Lorenz model by the $\hat{\theta}(0,0,2)$ mode:

$$j^{\rm conv}(t)\equiv(R_c^{\rm stat})^{-1}J^{\rm conv}(t)=2z(t)\ . \tag{A28}$$

For rigid boundaries the effective driving (A25) can be identified from the projection of the term $-u_3\partial_{x_3}T^{\rm cond}$ in Eq. (2.2b) onto the modes retained in θ. For the three-mode truncation of Gresho and Sani[17] discussed in Sec. II D this yields

$$\tilde{R}(t)=R(t)-(3\pi/4)\int_0^1 dx_3\sin^3(\pi x_3)\partial_{x_3}S^{\infty}(x_3,t)\ . \tag{A29}$$

Inserting (A4) into (A29) one obtains the temporal Fourier coefficients for the rigid case

$$\tilde{R}_\nu=R_\nu\left[\frac{9\pi^4}{(\pi^2-\gamma_\nu^2)(9\pi^2-\gamma_\nu^2)}\frac{\gamma_\nu/2}{\tan(\gamma_\nu/2)}\right]\ . \tag{A30}$$

APPENDIX B: BIFURCATION THRESHOLDS OF THE PERIODICALLY MODULATED OSCILLATOR

1. Numerical solution

The stability behavior of many parametrically modulated physical systems is that of the oscillator (3.1), which we rewrite as

$$m\ddot{x}+m\Gamma\dot{x}-[\epsilon+\tilde{\delta}c(\omega t)]x=0\ , \tag{B1}$$

i.e., as Hill's equation with damping. Unfortunately, the literature deals almost exclusively with the case of small damping, $\Gamma/\omega\ll 1$, whereas we are also interested in large Γ/ω (in the experiments described in paper II, Γ/ω went up to 20). Since the bifurcation thresholds of (B1) are of sufficient general interest we felt it worthwhile to investigate the stability behavior in some detail (see also Gresho and Sani[17]). We consider explicitly the case of a cosine modulation, $c(\omega t)=\cos(\omega t)$, and a step modulation $c(\omega t)=\mathrm{sgn}[\cos(\omega t)]$.

We first transform (B1) using

$$x(t)=y(\bar{\tau})\exp(-\bar{\tau}\Gamma/\omega),\quad \bar{\tau}=\omega t/2 \tag{B2}$$

into the standard form of a Mathieu or Hill equation

$$\left[\frac{d^2}{d\bar{\tau}^2}+a-2qc(2\bar{\tau})\right]y(\bar{\tau})=0\ , \tag{B3}$$

with

$$a=-\omega^{-2}(4\epsilon/m+\Gamma^2)\ , \tag{B4a}$$

$$q=2\tilde{\delta}/m\omega^2\ . \tag{B4b}$$

For temperature modulation $\tilde{\delta}$ is given by Eq. (3.6b), while for gravity modulation $\tilde{\delta}$ is replaced by the constant δ.

We look for the stability boundaries between the solution $x=0$ and a periodic Floquet solution[32]

$$x(t)=e^{(\mu-\Gamma/\omega)\bar{\tau}}P(\bar{\tau})\ . \tag{B5}$$

Since $P(\bar{\tau})=P(\bar{\tau}+\pi)$ is periodic (with the same period as the modulation) the bifurcation threshold is determined by the condition

$${\rm Re}\mu(a,q)=\Gamma/\omega\ , \tag{B6}$$

that the growth rate ${\rm Re}\mu$ of $y(\bar{\tau})=\exp(\mu\bar{\tau})P(\bar{\tau})$ should be just compensated by the damping rate Γ/ω. To evaluate the characteristic Floquet exponent $\mu(a,q)$ of the Mathieu equation we integrated (B3) from two different initial con-

ditions at $\bar{\tau}=0$ up to $\bar{\tau}=\pi/2$, as described by Abramowitz and Stegun.[33] The implicit equation (B6) has in general several solutions $a_c(q)$ for a fixed damping rate Γ/ω. Having found them, the stability boundaries are easily expressed with (B4) in terms of, e.g., ϵ and $\tilde{\delta}$.

In Fig. 9 we show the thresholds for harmonic and subharmonic bifurcations for various values of Γ/ω in the case of a cosine modulation. For ω,m,Γ fixed one can immediately translate the curves $a_c(q)$ of Fig. 9 into stability boundaries ϵ_c versus $\tilde{\delta}$: the point $-a_c(q\to 0)=\Gamma^2/\omega^2$ marks the zero of the ϵ axis for a particular damping Γ/ω since $q=0$ implies $\tilde{\delta}=0=\epsilon_c$. Note, furthermore, that small ω causes a, q, and $\mathrm{Re}\mu(a,q)=\Gamma/\omega$ to be large.

An analytic condition for the threshold in the limit $\omega\to 0$ then follows from the WKB expansion technique of Rosenblat and Herbert[7] or from the generalized asymptotic behavior of Mathieu functions used by Dowden.[15] The result is (see also Sec. III C)

$$\frac{\Gamma}{2}=\frac{1}{2\pi}\int_0^{2\pi} ds\left[\frac{\epsilon}{m}+\left[\frac{\Gamma}{2}\right]^2+\frac{\delta}{m}\cos s\right]^{1/2}, \tag{B7}$$

where $\delta=\tilde{\delta}(\omega=0)=r_0|\Delta|$.

2. Analytic theory for small modulation amplitude

Here we derive an analytic expression for the harmonic bifurcation threshold $\epsilon_c(\tilde{\delta},\omega)$ of (3.1) and (3.2) for sinusoidal and step modulations with small amplitudes $\tilde{\delta}\ll 1$. To that end we expand

$$\epsilon_c(\delta,\omega)=\epsilon_c^{(0)}+\tilde{\delta}\epsilon_c^{(1)}(\omega)+\tilde{\delta}^2\epsilon_c^{(2)}(\omega)+\cdots, \tag{B8}$$

as well as the periodic orbit

$$x(t)=x^{(0)}+\tilde{\delta}x^{(1)}(t)+\tilde{\delta}^2x^{(2)}(t) \tag{B9}$$

of Eq. (3.1) at threshold. The successive orders in $\tilde{\delta}$ yield the equations

$$L_0x^{(0)}(t)=0, \tag{B10a}$$

$$L_0x^{(1)}(t)=[\epsilon_c^{(1)}+c(\omega t)]x^{(0)}(t), \tag{B10b}$$

$$L_0x^{(2)}(t)=[\epsilon_c^{(1)}+c(\omega t)]x^{(1)}(t)+\epsilon_c^{(2)}x^{(0)}(t), \tag{B10c}$$

whose marginally stable (periodic) solutions we wish to find. Here L_0 is the operator

$$L_0=m\frac{d^2}{dt^2}+m\Gamma\frac{d}{dt}-\epsilon_c^{(0)}. \tag{B11}$$

Marginal stability of the solution of (B10a) implies the following condition on the characteristic exponents:

$$-\Gamma/2\pm(\Gamma^2/4+\epsilon_c^{(0)}/m)^{1/2}\le 0. \tag{B12}$$

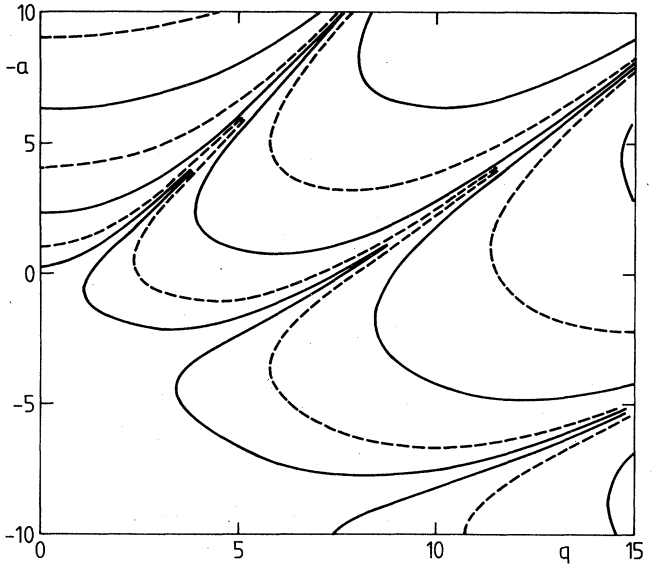

FIG. 9. Stability boundaries $a_c=-(4\epsilon_c/m+\Gamma^2)/\omega^2$ of the parametrically modulated damped oscillator as a function of $q=2\tilde{\delta}/m\omega^2$. Parabolic curves in the upper left-hand part denote thresholds for harmonic bifurcations for damping ratios Γ/ω increasing from 0.5 (bottom) to 3 (top) in steps of 0.5. They intersect the a axis at $-a_c(q=0)=\Gamma^2/\omega^2$. The adjacent tongue-shaped curves denote thresholds for subharmonic bifurcations for damping ratios increasing from 0.5 (lower left) to 2.5 (upper right) in steps of 0.5. The next set of tongues are thresholds for harmonic bifurcations for the same succession of damping ratios. Finally, the last three curves in the lower-right corner are again subharmonic thresholds for $\Gamma/\omega=0.5,1.0,1.5$. (Solid and dashed lines merely distinguish successive values of Γ/ω.)

Hence, $\epsilon_c^{(0)}=0$ and $x^{(0)}=\mathrm{const}$. The (solubility) condition that the solutions $x^{(1)}(t),x^{(2)}(t)$ are periodic requires the integrals of (B10b) and (B10c) over a whole period T to vanish. Therefore, $\epsilon_c^{(1)}=0$ and

$$\epsilon_c^{(2)}(\omega)=-T^{-1}\int_0^T dt\, c(\omega t)x^{(1)}(t)/x^{(0)}. \tag{B13}$$

For the sinusoidal modulation (3.3) the solution of (B10b) is

$$x^{(1)}(t)/x^{(0)}=-\frac{1}{m\omega}\mathrm{Re}\left[\frac{1}{\omega+i\Gamma}e^{-i\omega t}\right]. \tag{B14}$$

For the step modulation $x^{(1)}(t)/x^{(0)}$ is a lengthly expression which we do not write down explicitly. The threshold resulting from (B13) is then as shown in Eq. (3.10) of the text.

The precise domain of validity of these expressions is not immediately clear from an examination of the lowest-order expressions. One might think, for instance, that since Eq. (B14) behaves as ω^{-1} at $\omega t=\pi/2$ for small ω,

the domain of validity of the expansion (B8) and (B9) would be $\tilde{\delta}/\omega<1$ for $\omega\ll 1$. It turns out, however, that Eq. (3.10) is correct for $\tilde{\delta}\ll 1$, independent of $\tilde{\delta}/\omega$. A similar question arises in the nonlinear theory, as discussed in Appendix C.

3. Analytic theory for step modulation

The stability boundaries for the step modulation can be obtained analytically for arbitrary $\tilde{\delta}$ as follows:[14] The general solution of (B3) for $c(2\bar{\tau})=\mathrm{sgn}[\cos(2\bar{\tau})]$ is

$$y(\bar{\tau})=\begin{cases} A_1 e^{i\alpha\bar{\tau}}+A_2 e^{-i\alpha\bar{\tau}}, & \cos(2\bar{\tau})<0 \\ A_3 e^{i\beta\bar{\tau}}+A_4 e^{-i\beta\bar{\tau}}, & \cos(2\bar{\tau})>0 \end{cases} \tag{B15}$$

with

$$\alpha=\sqrt{a+2q}\,,\quad \beta=\sqrt{a-2q}\,. \tag{B16}$$

Continuity and periodicity of x and $\dot{x}$ yield four relations $(i=1,2,3,4)$ $\sum_{j=1}^{4}c_{ij}A_j=0$ between the amplitudes $\{A_j\}$, for which the solubility condition, $\det c_{ij}=0$, reads

$$\rho\cosh(\pi\Gamma/\omega)=\cos(\pi\alpha/2)\cos(\pi\beta/2) -[(\alpha^2+\beta^2)/2\alpha\beta] \times\sin(\pi\alpha/2)\sin(\pi\beta/2)\,. \tag{B17}$$

Here the solution of (B17) with $\rho=+1$ ($\rho=-1$) determines the threshold for a harmonic (subharmonic) bifurcation.

It may be shown that in the limit $\omega\to 0$ and for $\tilde{\delta}<m\Gamma^2/2$, Eq. (B17) implies

$$\epsilon_c(\tilde{\delta},\omega\to 0)=\frac{\tilde{\delta}^2}{m\Gamma^2}\left\{1+\frac{2\omega}{\pi\Gamma}\left[\left[\frac{m\Gamma^2}{2\tilde{\delta}}\right]^2-1\right] \times\ln\left[1-\left[\frac{2\tilde{\delta}}{m\Gamma^2}\right]^2\right]\right\}, \tag{B18}$$

which extends the result (3.10b) obtained from a small-$\tilde{\delta}$ expansion. The eigenfunctions of Eq. (B1) may be calculated for $\omega\to 0$ using a WKB approximation[34] as noted by Davis and Rosenblat.[19] Unfortunately, these authors did not carry out a consistent calculation, so we list here the full WKB answer, for $m=1$, $\Gamma=2$, and for the step modulation (3.4). The result is

$$x_1(t)=\begin{cases} e^{-t}(e^{(1+\tilde{\delta}/2)t}+\frac{1}{2}\tilde{\delta}e^{-(1+\tilde{\delta}/2)t}), & 0<\omega t\le\pi \\ e^{(2\pi/\omega)-t}[(1+\frac{1}{2}\tilde{\delta})e^{(1-\tilde{\delta}/2)(t-2\pi/\omega)}-\frac{1}{2}\tilde{\delta}e^{-(1-\tilde{\delta}/2)t}], & \pi<\omega t\le 2\pi\,. \end{cases} \tag{B19}$$

This function has discontinuities at both $\omega t=0$ and π, but these are small, i.e., of relative order $\exp(-\omega^{-1})$.

APPENDIX C: PERTURBATION EXPANSION

1. Anharmonic oscillator

We consider Eq. (4.1), which reads

$$m\ddot{x}+m\Gamma\dot{x}-\tilde{\epsilon}x+x^3=0\,, \tag{C1}$$

$$\tilde{\epsilon}=\epsilon+\tilde{\delta}c(\omega t)\,, \tag{C2}$$

where $c(\omega t)$ is any periodic function with period 2π, average zero, and maximum value unity.

a. Perturbation theory near threshold

To determine the small-norm periodic solutions near threshold we introduce an expansion parameter η [which will turn out to be proportional to $(\epsilon-\epsilon_c)^{1/2}$], and write

$$x(t)=\eta x_1(t)+\eta^2 x_2(t)+\eta^3 x_3(t)+\cdots\,, \tag{C3}$$

$$\epsilon=\epsilon_c(\omega,\tilde{\delta})+\eta\epsilon_1(\omega,\tilde{\delta})+\eta^2\epsilon_2(\omega,\tilde{\delta})+\cdots\,. \tag{C4}$$

Inserting these expansions into (C1) and equating like orders in η we obtain

$$\mathcal{L}_0 x_1\equiv m\ddot{x}_1+m\Gamma\dot{x}_1-[\epsilon_c+\tilde{\delta}c(\omega t)]x_1=0\,, \tag{C5a}$$

$$\mathcal{L}_0 x_2=\epsilon_1 x_1\,, \tag{C5b}$$

$$\mathcal{L}_0 x_3=\epsilon_2 x_1+\epsilon_1 x_2-x_1^3\,, \tag{C5c}$$

where $\mathcal{L}_0$ is analogous to L_0, Eq. (B11), except that in (C5a), $\epsilon_c(\tilde{\delta},\omega)$ is the exact threshold to all orders in $\tilde{\delta}$. The lowest-order equation is precisely Eq. (B1), discussed in Appendix B and the ensuing ϵ_c and x_1 can be obtained in general, though analytic expressions are only available for certain parameter regimes, such as $\tilde{\delta}\ll 1$, or $\omega\to 0$, or for certain functions $c(\tau)$. To solve the subsequent equations we define the eigenfunction $x_1^\dagger$ of the adjoint operator $\mathcal{L}_0^\dagger$ by

$$\mathcal{L}_0^\dagger x_1^\dagger\equiv m\ddot{x}_1^\dagger-m\Gamma\dot{x}_1^\dagger-[\epsilon_c+\tilde{\delta}c(\omega t)]x_1^\dagger=0\,, \tag{C6}$$

and take the scalar product of $x_1^\dagger$ with (C5b) and (C5c) over one period. We then find that $x_2=\epsilon_1=0$ and

$$\epsilon_2=\langle x_1^\dagger x_1^3\rangle/\langle x_1^\dagger x_1\rangle\,, \tag{C7a}$$

leading to the solution

$$x=\eta x_1=[(\epsilon-\epsilon_c)/\epsilon_2]^{1/2}x_1+O(\epsilon-\epsilon_c)\,. \tag{C7b}$$

Conditions for validity of the expansion are that $\eta\epsilon_3\ll\epsilon_2$, or $\eta^2 x_3\ll x_1$.

Let us apply the above results to the step modulation (3.4), for which the linear problem can be solved analytically for $\omega\to 0$ and $\tilde{\delta}<m\Gamma^2/2$. The result is Eq. (C7b) with ϵ_c and x_1 as calculated in Eqs. (B18) and (B19), respectively, and ϵ_2 is a constant we shall not evaluate explicitly. We now wish to ask over what range of parame-

ters the lowest-order solution (C7b) will be a good approximation to the exact answer. Davis and Rosenblat[19] determine this range by examining the ratio

$$\epsilon_2/\epsilon_c \propto \exp[(\pi\tilde{\delta}/\omega)-1] , \tag{C7c}$$

at fixed η, and imply that the expansion (C3) and (C4) breaks down for $\omega \ll \tilde{\delta}$ since ϵ_2/ϵ_c can become large. In fact, however, the quantity ϵ_2 depends on the arbitrary normalization chosen for the linear eigenfunctions x_1 and $x_1^\dagger$, whereas the more appropriate quantity [see Eq. (5.8) of Davis and Rosenblat[19]]

$$\eta^2\epsilon_2 = \epsilon - \epsilon_c \tag{C7d}$$

is independent of that normalization, and it does not diverge when $\omega \ll \tilde{\delta}$. By analogy to the case of the amplitude equation studied below, we conjecture that the limitation on the validity of the expansion does not come from Eq. (C4) for ϵ, but rather from Eq. (C3) for the function $x(t)$. This then suggests that Eq. (C7b) is a good approximation so long as $\epsilon-\epsilon_c \ll \omega$, independent of $\omega/\tilde{\delta}$. To test our conjecture we have integrated Eq. (C1) numerically with the step modulation (3.4) for $m=1$, $\Gamma=2$, and different values of ϵ, ω, and $\tilde{\delta}$. In each case we have compared the numerical results to Eqs. (C7b) and (B20) obtained using perturbation theory [since we did not evaluate the constant ϵ_2 in Eq. (C7b) we have fitted it by normalizing to the exact answer at $\omega t = 0.5$. We are thus testing only the shape of the solution and not its magnitude]. We consider three cases, the first two have $\epsilon-\epsilon_c < \omega$, and we expect perturbation theory to hold for these, whereas case (c) has $\epsilon-\epsilon_c > \omega$ and perturbation theory should break down. The results presented in Fig. 10 confirm our conjecture to reasonable accuracy. In particular, as long as $\epsilon-\epsilon_c \lesssim \omega$, the two curves agree for both $\omega < \tilde{\delta}$ [case (a)] and $\omega > \tilde{\delta}$ [case (b)]. This test shows that the relevant parameter for the validity of the perturbation expansion (C3) and (C4) is $(\epsilon-\epsilon_c)/\omega$ and not $\tilde{\delta}/\omega$, as implied by Davis and Rosenblat.[19]

It has already been remarked that for an arbitrary, i.e., non-step-wise modulation analytic expressions for the solutions x_1 and $x_1^\dagger$ of Eqs. (C5a) and (C6) are not available. Such solutions would determine via (C7a) and (C7b) the lowest-order bifurcating solution $x(t)$ above threshold,

$$x(t) = [\epsilon-\epsilon_c(\tilde{\delta},\omega)]^{1/2} f(t;\tilde{\delta},\omega) , \tag{C8a}$$

$$f(t;\tilde{\delta},\omega) = x_1(t)(\langle x_1 x_1^\dagger\rangle/\langle x_1^3 x_1^\dagger\rangle)^{1/2} . \tag{C8b}$$

If, however, $\tilde{\delta} \ll 1$ and $\tilde{\delta}/\omega \ll 1$ one can expand x_1, $x_1^\dagger$, and $\tilde{\epsilon}_c$ in $\tilde{\delta}$,

$$x_1(t;\tilde{\delta}) = 1+\tilde{\delta}x_1^{(1)}(t)+\tilde{\delta}^2 x_1^{(2)}(t)+\cdots , \tag{C9a}$$

$$x_1^\dagger(t;\tilde{\delta}) = 1+\tilde{\delta}x_1^{\dagger(1)}(t)+\tilde{\delta}^2 x_1^{\dagger(2)}(t)+\cdots , \tag{C9b}$$

$$\epsilon_c(\tilde{\delta}) = \tilde{\delta}^2\epsilon_c^2+\cdots .$$

Here we have used the fact that the dummy constants $x_1^{(0)}$ and $x_1^{\dagger(0)}$ drop out of (C8) and therefore may be set equal to 1 for convenience. Inserting the small-$\tilde{\delta}$ expansion into (C5a) one obtains the sequence (B10) of linear equations with constant coefficients and a similar sequence with Γ replaced by $-\Gamma$ from (C6). These equations can be solved for any modulation.[30]

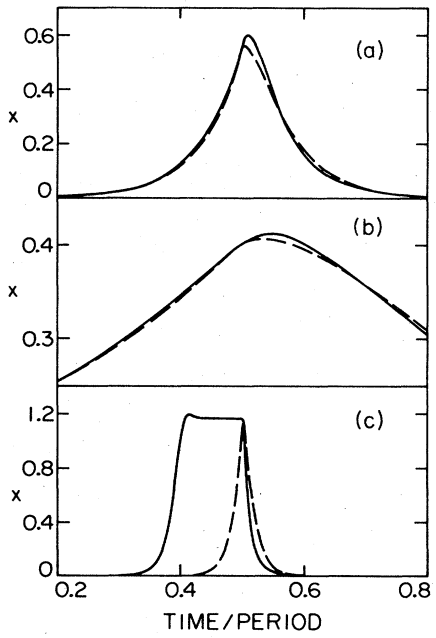

FIG. 10. Time dependence of solutions of the parametrically modulated nonlinear oscillated (C1) with the step modulation (3.4) for $m=1$, $\Gamma=2$, and various values of ω, $\tilde{\delta}$, and ϵ. Solid curves are numerical solutions of the nonlinear equation, and the dashed curves are calculated from first-order perturbation theory [Eqs. (B19) and (B20)]. Solutions are periodic in the interval $0 < \omega t/2\pi \leq 1$, and the dashed curve was fitted to the solid curve at $\omega t/2\pi = 0.5$. (a) $\omega=0.2$, $\tilde{\delta}=1$, $\epsilon=0.266$ so $\epsilon-\epsilon_c=0.03$. (b) $\omega=1$, $\tilde{\delta}=0.5$, $\epsilon=0.144$ so $\epsilon-\epsilon_c=0.1$. (c) $\omega=0.05$, $\tilde{\delta}=1$, $\epsilon=0.357$, so $\epsilon-\epsilon_c=0.11$.

For a sinusoidal modulation, $c(\omega t)=\cos(\omega t)$, the lowest-order result has been given in (B14). The next order reads

$$x_1^{(2)}(t) = \left[\frac{1}{2m\omega}\right]^2 \mathrm{Re}\left[\frac{1}{\omega+i\Gamma}\frac{1}{2\omega+i\Gamma}e^{-i2\omega t}\right] , \tag{C10a}$$

and to obtain $x_1^{\dagger(n)}$ one has to replace Γ by $-\Gamma$ in $x_1^{(n)}$. Inserting the above results into (C8b) one obtains

$$f(t;\tilde{\delta},\omega) = \left[1-\frac{1}{4}\left[\frac{\tilde{\delta}}{m\omega}\right]^2\frac{5\omega^2+\Gamma^2}{(\omega^2+\Gamma^2)^2}+O(\tilde{\delta}^4)\right]$$

$$\times[1+\tilde{\delta}x_1^{(1)}(t)+\tilde{\delta}^2 x_1^{(2)}(t)+O(\tilde{\delta}^3)] . \tag{C10b}$$

It is now a simple matter to evaluate the slope s of Eq. (4.6b) from (C8) and (C10b), and the result is given in Eq. (4.7).

b. Adiabatic expansion above threshold

If the function $\tilde{\epsilon}(t)$, Eq. (C2), remains positive for the whole period (i.e., $\epsilon > \tilde{\delta}$), then there exists an adiabatic expansion for small ω, which we now discuss. Let us divide the time dependence of $x(t)$ into a rapid variation with

variable t_1 and a slow variation with variable $\tau=\omega t$, coming from the dependence on $\tilde{\epsilon}(\tau)$. (In this appendix we use the variable $\tau=\omega t$, as contrasted with $\bar{\tau}=\omega t/2$ used in Appendix B.) Then the time derivatives in Eq. (C1) become

$$\partial_t=\partial_{t_1}+\omega\partial_\tau\ , \tag{C11}$$

and we shall expand the quantities in (C1) in ω, considering τ derivatives to be of order unity. Let

$$x(t)=x^{(0)}(t_1,\tilde{\epsilon}(\tau))+\omega x^{(1)}(t_1,\tilde{\epsilon}(\tau)) +\omega^2 x^{(2)}(t_1,\tilde{\epsilon}(\tau))+\cdots\ . \tag{C12}$$

In steady state (i.e., $t_1\to\infty$) we can neglect the dependence on t_1. Inserting (C12) into the equation of motion (C1) we obtain equations in the variable τ at each order in ω:

$$-\tilde{\epsilon}x^{(0)}+(x^{(0)})^3=0\ , \tag{C13a}$$

$$m\Gamma\partial_\tau x^{(0)}-\tilde{\epsilon}x^{(1)}+3(x^{(0)})^2x^{(1)}=0\ , \tag{C13b}$$

$$m\partial_\tau^2 x^{(0)}+m\Gamma\partial_\tau x^{(1)}-\tilde{\epsilon}x^{(2)}+3x^{(0)}(x^{(1)})^2 +3(x^{(0)})^2x^{(2)}=0\ , \tag{C13c}$$

leading to the adiabatic solution

$$x(\omega t=\tau)=\tilde{\epsilon}^{1/2}-\frac{\omega m\Gamma}{4\tilde{\epsilon}^{3/2}}\tilde{\epsilon}' +\frac{m\omega^2}{4\tilde{\epsilon}^{3/2}}\left[\left[1-\frac{9m\Gamma^2}{4\tilde{\epsilon}}\right]\frac{(\tilde{\epsilon}')^2}{2\tilde{\epsilon}} -\left[1-\frac{m\Gamma^2}{2\tilde{\epsilon}}\right]\tilde{\epsilon}''\right]+O(\omega^3)\ , \tag{C14}$$

where the prime denotes differentiation with respect to τ.

2. Amplitude equation

The perturbative techniques discussed in the previous section may also be applied to the first-order amplitude equation (4.2)

$$\dot{x}(t)-\tilde{\epsilon}(t)x(t)+x^3(t)=0\ , \tag{C15}$$

where $\tilde{\epsilon}$ is still given by (C2). This equation has the advantage that the periodic solutions can be written down in quadratures[23] as

$$x^2(\tau)=\frac{\omega}{2}\frac{[\psi(2\pi)-1]\psi(\tau)}{2\pi\langle\psi\rangle+[\psi(2\pi)-1]\int_0^\tau\psi(\tau')d\tau'}\ , \tag{C16}$$

where

$$\psi(\tau)=\exp\left[2\int_0^\tau\tilde{\epsilon}(\tau')d\tau'\right]\ , \tag{C17a}$$

$$\langle\psi\rangle\equiv(2\pi)^{-1}\int_0^{2\pi}\psi(\tau')d\tau'\ . \tag{C17b}$$

We shall obtain solutions of (C15) by expansion techniques and compare to the exact result (C16) in order to determine the range of validity of the expansions.

a. Perturbation theory near threshold

The perturbation technique of Davis and Rosenblat[19] is very simple to apply to the present equation (for which $\epsilon_c\equiv 0$), and we find for a cosine modulation

$$x^2(\tau)=\epsilon[I_0(2\tilde{\delta}/\omega)]^{-1}\exp[(2\tilde{\delta}/\omega)\sin\tau]+O(\epsilon^2)\ , \tag{C18}$$

where I_0 is a Bessel function.[33] It is now interesting to inquire firstly whether the above expression is valid for all $\omega/\tilde{\delta}$, and secondly what the form of the $O(\epsilon^2)$ corrections is. Turning to the exact expression (C16) for a cosine modulation, we note that for $\epsilon/\omega\ll 1$ with $\omega/\tilde{\delta}$ arbitrary we may write

$$\psi(\tau)=\phi(\tau)\exp[(2\epsilon/\omega)\tau] =\phi(\tau)(1+2\epsilon\tau/\omega+2\epsilon^2\tau^2/\omega^2+\cdots) \tag{C19}$$

with

$$\phi(\tau)\equiv\exp[(2\tilde{\delta}/\omega)\sin\tau]\ . \tag{C20}$$

Inserting this expansion into (C16) we find

$$x^2(\tau)=\epsilon\chi(\tau)\left[1+(2\epsilon/\omega)\left[\pi+\tau-\langle\tau\chi\rangle-\int_0^\tau\chi(\tau')d\tau'\right]+O(\epsilon^2/\omega^2)\right]\ , \tag{C21}$$

where $\chi(\tau)\equiv\phi(\tau)/\langle\phi\rangle$. The first term on the rhs of (C21) is precisely (C18), the perturbation result, and the second term in the large square brackets clearly remains bounded when $\tilde{\delta}/\omega\to\infty$, so that it represents a small correction when $\epsilon/\omega\ll 1$. [It is easy to verify that (C21) is periodic in τ, and that the sum rule (3.7) is exhausted by the lowest term, i.e., that the $O(\epsilon^2)$ term integrates to zero.] The present calculation thus shows that perturbation theory is valid in the range $\epsilon\ll\omega\ll\tilde{\delta}$, even though the function (C18) has a very sharp peak. A similar discussion can be given for other functions $c(\tau)$, for instance for a step.

In the range $\omega\ll\epsilon<\tilde{\delta}$ in which perturbation theory breaks down, we have not found any significant simplification of the exact expression (C16), valid uniformly over the whole range of τ.

b. Adiabatic expansion above threshold

For the case $\epsilon>\tilde{\delta}$ ($\tilde{\epsilon}>0$) and $\omega\to 0$ the adiabatic expansion can also be applied to Eq. (C15) and we find

$$x(\tau)=\tilde{\epsilon}^{1/2}-\frac{\omega\tilde{\epsilon}'}{4\tilde{\epsilon}^{3/2}}-\frac{\omega^2}{8\tilde{\epsilon}^{5/2}}\left[\frac{9(\tilde{\epsilon}')^2}{4\tilde{\epsilon}}-\tilde{\epsilon}''\right]+O(\omega^3)\ , \tag{C22}$$

which agrees with (C14) in the limit $m\to 0$, $m\Gamma\to 1$. We may check the validity of this expansion by examining Eq. (C16) for $\omega\ll\tilde{\delta}<\epsilon$. Let us consider the cosine modulation, for which the integral in (C16) can be evaluated by a saddle-point method

$$\int_0^\tau \psi(\tau')d\tau' \approx \phi(\tau)\exp(2\epsilon\tau/\omega)\frac{1-\exp(-2\tilde{\epsilon}\tau/\omega)}{2\tilde{\epsilon}/\omega}\ ,$$
$$\omega \ll \tilde{\delta} \ll \epsilon\ . \quad \text{(C23)}$$

Inserting this expression into (C16), we find

$$x^2(\tau)=\tilde{\epsilon}(\tau)[1+O(\omega/\tilde{\epsilon})]\ , \quad \text{(C24)}$$

in agreement with (C22). Note, however, that there are also nonanalytic corrections containing factors $\exp(-2\epsilon\tau/\omega)$ which are missed in the adiabatic expansion (C22).

3. Lorenz model

Here we shall outline the perturbation theory for the bifurcating solution

$$X(t)=(x(t),y(t),z(t)) \quad \text{(C25)}$$

of the Lorenz model (2.7) immediately above the threshold ϵ_c. With the expansion

$$X(t)=\eta X_1(t)+\eta^2 X_2(t)+\cdots\ , \quad \text{(C26)}$$

$$\epsilon-\epsilon_c=\eta\epsilon_1+\eta^2\epsilon_2+\cdots\ , \quad \text{(C27)}$$

the nonlinear system of differential equations (2.7) is transformed into a sequence of linear problems. For temperature as well as for gravity modulation one finds from the first order in η that

$$z_1(t)=0=z_1^\dagger(t)\ , \quad \text{(C28)}$$

while $x_1,y_1,x_1^\dagger,y_1^\dagger$ are all finite. To second order in η one obtains

$$(\tau_1\partial_t+b)z_2(t)=bx_1(t)y_1(t)\ , \quad \text{(C29)}$$

and

$$\epsilon_1=0\ , \quad \text{(C30)}$$

and the third-order equation yields ϵ_2 in terms of x_1 and $x_1^\dagger$.

While the above equations (C25)–(C30) hold for temperature and gravity modulation, the functions $X_1(t)$ and $X_1^\dagger(t)$ given below and the thresholds ϵ_c are different for the two modulation procedures. The bifurcating solution $z(t)$ which determines the convective current is given in each case to lowest order in $\epsilon-\epsilon_c$ by

$$z(t)=\eta^2 z_2(t)=(\epsilon-\epsilon_c)z_2(t)/\epsilon_2\ . \quad \text{(C31)}$$

Its mean may thus be written as

$$\langle z(t)\rangle=(\epsilon-\epsilon_c)s\ , \quad \text{(C32a)}$$

with a slope

$$s=\langle z_2\rangle/\epsilon_2\ . \quad \text{(C32b)}$$

a. Temperature modulation

For temperature modulation the first order in η yields in addition to (C28) the following four equations for the functions $x_1,y_1,x_1^\dagger,y_1^\dagger$:

$$[m\partial_t^2+m\Gamma\partial_t-\epsilon_c^T(\delta,\omega)-\tilde{\delta}\cos(\omega t)]x_1(t)=0\ , \quad \text{(C33a)}$$

$$y_1(t)=[(\tau_1/\tilde{\sigma})\partial_t+1]x_1(t)\ , \quad \text{(C33b)}$$

$$[m\partial_t^2-m\Gamma\partial_t-\epsilon_c^T(\delta,\omega)-\tilde{\delta}\cos(\omega t)]y_1^\dagger(t)=0\ , \quad \text{(C33c)}$$

$$x_1^\dagger(t)=\tilde{\sigma}^{-1}(1-\tau_1\partial_t)y_1^\dagger(t)\ . \quad \text{(C33d)}$$

Here $m=(\tau_1)^2/\tilde{\sigma}$, (2.19); $\Gamma=(\tilde{\sigma}+1)/\tau_1$, (2.20); $\tilde{\delta}=\delta\,|\,\tilde{\Delta}/\Delta\,|$, (3.6); and $\epsilon_c^T(\delta,\omega)$ is given up to second order in δ in (3.11). The solvability condition in order η^3 yields

$$\epsilon_c=\langle y_1^\dagger x_1 z_2\rangle/\langle y_1^\dagger x_1\rangle\ . \quad \text{(C34)}$$

For small-modulation amplitude one may solve (C33) analytically via a δ expansion (cf. Sec. 1 of this Appendix). Having determined $x_1,y_1,y_1^\dagger$ and with it also z_2, (C29), one has all the necessary ingredients to evaluate the bifurcating solution $z(t)$ in (C31) for small δ. The calculation is straightforward but somewhat cumbersome. Since the small-δ solution of (C33a) and (C33c) has been given already in Sec. 1 of this Appendix we do not write down $z(t)$ explicitly. We only remark that to evaluate the growth coefficient (C32b) of $\langle z(t)\rangle$ up to second order in δ one needs x_1, y_1, and $y_1^\dagger$ to first order only. The result is given in Eq. (4.9)

b. Gravity modulation

In this case, [Eq. (2.33)] the first-order equations read

$$[m\partial_t^2+m\Gamma\partial_t-\epsilon_c^G(\delta,\omega)-\delta\cos(\omega t)]y_1(t)=0\ , \quad \text{(C35a)}$$

$$[1+\epsilon_c^G(\delta,\omega)]x_1(t)=(1+\tau_1\partial_t)y_1(t)\ , \quad \text{(C35b)}$$

$$[m\partial_t^2-m\Gamma\partial_t-\epsilon_c^G(\delta,\omega)-\delta\cos(\omega t)]x_1^\dagger(t)=0\ , \quad \text{(C35c)}$$

$$y_1^\dagger(t)=(\tilde{\sigma}-\tau_1\partial_t)x_1^\dagger(t)\ , \quad \text{(C35d)}$$

with $\epsilon_c^G(\delta,\omega)$ given up to second order in δ by (3.20). The solvability condition yields

$$\epsilon_2=\langle y_1^\dagger x_1 z_2\rangle\langle y_1^\dagger x_1-x_1^\dagger[(\tilde{\sigma}+\tau_1\partial_t)x_1-\tilde{\sigma}y_1]\rangle^{-1}\ . \quad \text{(C36)}$$

Using (C35b) one finds for the growth coefficient (C32b)

$$s_G(\delta,\omega)=\langle y_1^\dagger x_1-\tilde{\sigma}\delta[1+\epsilon_c^G(\delta,\omega)]^{-1}x_1^\dagger y_1\cos(\omega t)\rangle \times\langle z_2\rangle/\langle y_1^\dagger x_1 z_2\rangle\ , \quad \text{(C37)}$$

which can be evaluated in the same way as for temperature modulation, and the result is given in Eq. (4.10).

APPENDIX D: EFFECT OF SIDEWALLS

1. Conductive temperature profile

Here we solve the heat conduction equation for the fluid layer described in Sec. I, but with the addition of lateral sidewalls perpendicular to the $\hat{x}_1$ direction. The walls extend from $x_1=\pm L$ to $x_1=\pm(L+t_w)$ where t_w is the wall thickness (in units of d). As in Appendix A we consider the general case in which periodically varying temperatures are imposed at the top, $x_3=1$,

$$T^u(t)=\sum_{\nu=-\infty}^{\infty} T_\nu^u e^{-i\omega\nu t}\ , \quad \text{(D1)}$$

and at the bottom, $x_3=0$, according to

$$T^l(t)-T^u(t)=R(t)=\sum_{\nu=-\infty}^{\infty} R_\nu e^{-i\omega\nu t} . \tag{D2}$$

We write the resulting temperature field

$$T^{\rm cond}(x_1,x_3,t)=T^u(t)+R(t)(1-x_3)+S(x_1,x_3,t) , \tag{D3}$$

as a linear profile plus a deviation

$$S(x_1,x_3,t)=\sum_{\nu=-\infty}^{\infty} S_\nu(x_1,x_3)e^{-i\omega\nu t} \tag{D4}$$

depending here also on x_1 due to the presence of the sidewalls. Obviously $S=0$ at $x_3=0,1$. In addition we require the following boundary conditions for S: (i) no heat current leaves the system through the outer wall boundaries at $x_1=\pm(L+t_w)$ (this condition is very well realized in the experimental setup of paper II); (ii) S is continuous across the inner wall boundary at $x_1=\pm L$; (iii) the horizontal heat current across $x_1=\pm L$ is continuous.

It is convenient to solve the heat equation in terms of the modes

$$S_\nu(x_1,n_3)=-\int_0^1 dx_3 S_\nu(x_1,x_3)\sin(n_3\pi x_3) , \tag{D5}$$

entering the Fourier series expansion of S with respect to the $\hat{\mathbf{x}}_3$ direction. A straightforward, somewhat lengthy, calculation yields for the deviation from the linear profile *in the fluid* $(-L\le x_1\le L)$

$$S_\nu(x_1,n_3)=S_\nu^\infty(n_3)\left[1-\phi_\nu(n_3)\frac{\cosh[\Omega_\nu(n_3)x_1]}{\cosh[\Omega_\nu(n_3)L]}\right] , \tag{D6}$$

with

$$\Omega_\nu^2(n_3)=n_3^2\pi^2-i\omega\nu . \tag{D7}$$

Note that the modulation frequency ω is measured in units of the vertical diffusion time of the fluid. In Eq. (D6)

$$S_\nu^\infty(n_3)=-i\omega\nu R_\nu\frac{1+[1-(-1)^{n_3}]T_\nu^u/R_\nu}{\pi n_3\Omega_\nu^2(n_3)} \tag{D8}$$

is the solution in the absence of sidewalls, $L=\pm\infty$. One can easily verify that (D8) is the Fourier transform of $S_\nu^\infty(x_3)$, Eq. (A4). The quantity

$$\phi_\nu(n_3)=(1-\lambda_1)\frac{\pi^2 n_3^2}{\overline{\Omega}_\nu^2(n_3)}\times\left[1+\lambda_2\frac{\Omega_\nu(n_3)}{\overline{\Omega}_\nu(n_3)}\frac{\tanh[\Omega_\nu(n_3)L]}{\tanh[\overline{\Omega}_\nu(n_3)t_w]}\right]^{-1} \tag{D9}$$

involves the ratios λ_1 and λ_2 defined in Eq. (5.4b), and

$$\overline{\Omega}_\nu^2(n_3)=\pi^2 n_3^2-i\omega\nu\lambda_1 . \tag{D10}$$

The change

$$S_\nu^w(x_1,n_3)=S_\nu(x_1,n_3)-S_\nu^\infty(n_3)=-S_\nu^\infty(n_3)\phi_\nu(n_3)\frac{\cosh[\Omega_\nu(n_3)x_1]}{\cosh[\Omega_\nu(n_3)L]} \tag{D11}$$

of the temperature profile in the fluid caused by the presence of the walls is of relative size $-\phi_\nu(n_3)$ at $x_1=\pm L$, and decays inwards towards $x_1=0$ to the value $-\phi_\nu(n_3)/\cosh[\Omega_\nu(n_3)L]$ with a decay length $1/\mathrm{Re}[\Omega_\nu(n_3)]$ describing the penetration depth of heat "waves" entering the fluid from the sidewalls. This penetration depth is for all frequencies less than $(\pi n_3)^{-1}$.

For the subsequent analysis we need the Fourier mode

$$\hat{S}_\nu^w(n_1,0,n_3)=\frac{1}{2L}\int_{-L}^{L} dx_1 e^{-ik_1x_1n_1}S_\nu^w(x_1,n_3) \tag{D12}$$

$$=-S_\nu^\infty(n_3)\phi_\nu(n_3)\frac{1}{L}\frac{k_1n_1\sin(k_1n_1L)+\Omega_\nu(n_3)\cos(k_1n_1L)\tanh[\Omega_\nu(n_3)L]}{k_1^2n_1^2+\Omega_\nu^2(n_3)} \tag{D13}$$

at the critical wave number $k_1=k_c$ (which for free boundary conditions is $k_c=\sqrt{\pi}/2$). Note that for $\mathrm{Re}[\Omega_\nu(n_3)]L\gg 1$, $\tanh[\Omega_\nu(n_3)L]$ may be replaced by 1.

2. Sidewall forcing

The above modes (D13) modify the Lorenz truncation (A17) of the Boussinesq equations as follows:

$$\partial_t\hat{u}_1(1,0,1)=-\sigma(k_1^2+\pi^2)\hat{u}_1(1,0,1)-\sigma[k_1\pi/(k_1^2+\pi^2)][\hat{\theta}(1,0,1)+\hat{S}_w(1,0,1)] , \tag{D14a}$$

$$\partial_t\hat{\theta}(1,0,1)=-(k_1^2+\pi^2)\hat{\theta}(1,0,1)-(k_1/\pi)\hat{u}_1(1,0,1)[R-2\pi\hat{S}^\infty(2)-2\pi\hat{\theta}(0,0,2)-2\pi\hat{S}_w(0,0,2)] , \tag{D14b}$$

$$\partial_t\hat{\theta}(0,0,2)=-4\pi^2\hat{\theta}(0,0,2)-4k_1\hat{u}_1(1,0,1)[\hat{\theta}(1,0,1)+\hat{S}_w(1,0,1)], \tag{D14c}$$

where we have suppressed the time variable in all quantities. In case of an out-of-phase modulation of the temperatures of the top and bottom plates according to $T_\nu^u=-\frac{1}{2}R_\nu$ $(\nu\ge 1)$ the wall contribution $\hat{S}_w$ vanishes for all odd n_3 due to Eqs. (D8), (D1), and (D2). Therefore the sidewall effect enters into the Lorenz model in that case only multiplicatively via $\hat{S}_w(0,0,2)$ in (D14b). If, however, only the bottom temperature is modulated, $T_\nu^u=0$ $(\nu\ge 1)$, the sidewall terms $\hat{S}_w$ modify the Lorenz model additively as well as multiplicatively.

Equations (D14) are now written in the form (2.7), where we retain $\hat{S}_w$ only in (D14a) where it appears as an additive contribution which modifies (2.7a) to (5.2). [We

neglect the multiplicative effects of $\hat{S}_w$ in (D14b) and (D14c)]. The forcing term is

$$\xi(t)=\sqrt{3}\pi\hat{S}_w(1,0,1;t)/R_c^{\rm stat} . \tag{D15}$$

Its Fourier amplitudes

$$\xi_\nu=-i\omega\nu\frac{T_\nu^l+T_\nu^u}{R_c^{\rm stat}}\tilde{\psi}(\omega\nu) \tag{D16}$$

may be written according to (D8), (D12), and (D13) in terms of the function

$$\tilde{\psi}(\omega\nu)=-\frac{\sqrt{3}}{L}\frac{k_c\sin(k_cL)+\Omega_\nu\cos(k_cL)}{\Omega_\nu^2(\Omega_\nu^2+k_c^2)}\phi_\nu(n_3=1) , \tag{D17}$$

where $\Omega_\nu=\Omega_\nu(n_3=1)$. The quantity f (5.4) is just the zero-frequency limit of (D17), $f=\tilde{\psi}(0)$, which may be verified with the help of (D7), (D9), and (D10). Thus (D16) has the form (5.3) with

$$\psi(\omega\nu)=\tilde{\psi}(\omega\nu)/\tilde{\psi}(0) . \tag{D18}$$

Another form for ξ at finite frequency is suggested by the analysis in Eqs. (32) and (33) of Cross *et al.*,[22] which is consistent with the amplitude equation, namely

$$\xi(t)=f\dot{r}(t)\{1+\bar{\epsilon}_c^{-1}[r(t)-1]\} , \tag{D19}$$

$$\bar{\epsilon}_c=\xi_c^2\pi^2/4L^2=2/3L^2 . \tag{D20}$$

---

*Permanent address.

[1]R. J. Donnelly, F. Reif, and H. Suhl, Phys. Rev. Lett. **9**, 363 (1962).

[2]R. J. Donnelly, Proc. R. Soc. London Ser. A **281**, 130 (1964).

[3]G. Ahlers, P. C. Hohenberg, and M. Lücke, following paper, Phys. Rev. A **32**, 3519 (1985). Referred to as paper II.

[4]S. H. Davis, Annu. Rev. Fluid Mech. **8**, 57 (1976).

[5]R. G. Finucane and R. E. Kelly, Int. J. Heat Mass Transfer **19**, 71 (1976).

[6]J. P. Gollub and S. V. Benson, Phys. Rev. Lett. **41**, 948 (1978).

[7]S. Rosenblat and D. M. Herbert, J. Fluid Mech. **43**, 385 (1970).

[8]E. N. Lorenz, J. At. Sci. **20**, 130 (1963).

[9]J. B. McLaughlin and P. C. Martin, Phys. Rev. A **12**, 186 (1975).

[10]G. Ahlers, P. C. Hohenberg, and M. Lücke, Bull. Am. Phys. Soc. **26**, 1271 (1981).

[11]G. Ahlers, P. C. Hohenberg, and M. Lücke, Phys. Rev. Lett. **53**, 48 (1984).

[12]M. N. Roppo, S. H. Davis, and S. Rosenblat, Phys. Fluids **27**, 796 (1984).

[13]V. Steinberg, G. Ahlers, and D. S. Cannell (unpublished).

[14]G. Z. Gershuni and E. M. Zhukhovitskii, *Convective Stability of Incompressible Fluids,* translated by D. Louvish (Keter, Jerusalem, 1976).

[15]J. Dowden, J. Fluid Mech. **110**, 149 (1981).

[16]G. Venezian, J. Fluid Mech. **35**, 243 (1969).

[17]P. M. Gresho and R. L. Sani, J. Fluid Mech. **40**, 783 (1970).

[18]S. Rosenblat and G. A. Tanaka, Phys. Fluids **14**, 1319 (1971).

[19]S. H. Davis and S. Rosenblat, Stud. Appl. Math. **57**, 59 (1977).

[20]S. H. Davis, J. Fluid Mech. **45**, 33 (1970).

[21]G. Ahlers, M. C. Cross, P. C. Hohenberg, and S. Safran, J. Fluid Mech. **110**, 297 (1981).

[22]M. C. Cross, P. C. Hohenberg, and M. Lücke, J. Fluid Mech. **136**, 269 (1983).

[23]P. Hall, J. Fluid Mech. **67**, 29 (1975).

[24]K. Takeyama, Prog. Theor. Phys. **63**, 91 (1980).

[25]A. C. Newell and J. A. Whitehead, J. Fluid Mech. **38**, 279 (1969).

[26]J. Wesfreid, Y. Pomeau, M. Dubois, C. Normand, and P. Bergé, J. Phys. (Paris) Lett. **39**, 725 (1978).

[27]M. C. Cross, Phys. Fluids **23**, 1727 (1980).

[28]In our earlier work (Ref. 11) we introduced a "phenomenological" rigid model given by Eqs. (2.7) and (2.14)–(2.16) with $\tau_1=\tau_1^f(\tau_0^r)_{\rm ex}/\tau_0^f$, $g=(g_r)_{\rm ex}$, $\tilde{\sigma}=\sigma_f$, $b=b_f$, $\tilde{r}=\tilde{r}_f$. Although the quantitative predictions of this model are very close to those of the model based on (2.32) we use here, we prefer the latter from a logical point of view since the only approximation made is the three-mode truncation.

[29]I. S. Gradshteyn and I. M. Ryzhik, *Table of Integrals, Series and Products* (Academic, New York, 1981).

[30]M. Lücke and F. Schank, Phys. Rev. Lett. **54**, 1465 (1985).

[31]The constant f defined in Eq. (5.3) is related to the corresponding quantity $\bar{f}^1$ of Eq. (4.24) of Ref. 21 and Eq. (37) of Ref. 22 by a constant normalization factor, $f=\tau_0 g^{1/2}\bar{f}^1$. In Ref. 11 the value $f=0.04$ quoted for the fit in Fig. 1 was actually the numerical value of $\bar{f}^1$. The corresponding value for f is 4.5×10^{-3}.

[32]E. A. Coddington and N. Levinson, *Theory of Ordinary Differential Equations* (McGraw-Hall, New York, 1978).

[33]*Handbook of Mathematical Functions,* edited by M. Abramowitz and I. A. Stegun (Dover, New York, 1965).

[34]C. M. Bender and S. A. Orszag, *Advanced Mathematical Methods for Scientists and Engineers* (McGraw-Hill, New York, 1978).